BRAIN
ORIGINAL ARTICLE

Inhibition of GluN2B-containing N-methyl-D-aspartate receptors by radiprodil

Tue G. Banke,[1] Michael C. Regan,[2] Riley E. Perszyk,[1] Lu Zhang,[1,†] Hao Xing,[1] Jiahui Chen,[3] Sehoon Won,[4] Noriko Simorowski,[2] Eva S. Diaz,[1] Sukhan Kim,[1,5] Rui Song,[1,‡] Jian Rong,[3] Xin Zhou,[3] Ahmad F. Chaudhary,[3] Jing Zhang,[1] John F. Traynelis,[1] Ellington D. McDaniels,[1] Karolina Nitsche,[6] Steve Roache,[6] Christopher S. Raymond,[6] Chian-Ming Low,[7] Scott J. Myers,[1,5] Katherine W. Roche,[4] Steven H. Liang,[3] Stephen F. Traynelis,[1,5,8] Hiro Furukawa[2] and Hongjie Yuan[1,5]

N-methyl-D-aspartate (NMDA) receptors mediate a slow, Ca^{2+}-permeable component of excitatory synaptic transmission in the brain and participate in neuronal development and synaptic plasticity. Most NMDA receptors are tetrameric assemblies of two GluN1 and two GluN2 subunits encoded by five genes (*GRIN1* and *GRIN2A–GRIN2D*), which produce GluN1 and GluN2A–GluN2D subunits. NMDA receptors that contain the GluN2B subunit have unique pharmacological properties, being inhibited by multiple structurally distinct series of biaryl compounds with high potency and selectivity. These agents are of considerable therapeutic interest, given the numerous roles that GluN2B-containing NMDA receptors play in normal brain function and pathological situations.

Among GluN2B-selective negative allosteric modulators, radiprodil inhibits NMDA receptors that contain GluN2B with high potency and selectivity and appears to be safe in humans. Here, we evaluate the structural determinants of radiprodil binding to the heterodimeric GluN1–GluN2B amino terminal domain by X-ray crystallography and explore the molecular mechanism of inhibition. A large number of *de novo* variants have been identified in the *GRIN* gene family in patients with various neurological and neuropsychiatric conditions, including autism, intellectual disability, epilepsy, language disorders and movement disorders. We show that radiprodil is an effective antagonist at >80% of human disease-associated *GRIN1* and *GRIN2B* missense variants tested *in vitro* (22/27, equally or more effective as wild-type receptors), including variants in the pore-forming region, linker regions and elsewhere that uniformly increase NMDA receptor-mediated charge transfer. We show that radiprodil blocks synaptic GluN2B receptors in brain slices acutely isolated from a knock-in mouse line harbouring the gain-of-function variant GluN2B-Ser810Arg associated with early-onset epileptic encephalopathy and intractable seizures in patients. In addition, radiprodil delays the onset of seizures (458 ± 90 s, versus 207 ± 23 s in the vehicle group) in response to *in vivo* administration of the chemoconvulsant pentylenetetrazole.

These data support the potential utility of GluN2B-selective antagonists, such as radiprodil, for clinical treatments of neurological conditions where clinical aetiologies might involve increased current mediated by GluN2B-containing NMDA receptors.

1 Department of Pharmacology and Chemical Biology, Emory University School of Medicine, Atlanta, GA 30322, USA
2 W.M. Keck Structural Biology Laboratory, Cold Spring Harbor Laboratory, New York, NY 11724, USA
3 Department of Radiology and Imaging Sciences, Emory University, Atlanta, GA 30322, USA
4 Receptor Biology Section, National Institute of Neurological Disorders and Stroke (NINDS), National Institutes of Health (NIH), Bethesda, MD 20892, USA
5 Center for Functional Evaluation of Rare Variants (CFERV), Emory University School of Medicine, Atlanta, GA 30322, USA

Received February 28, 2025. Revised August 20, 2025. Accepted August 29, 2025. Advance access publication September 25, 2025
Published by Oxford University Press on behalf of the Guarantors of Brain 2025.

6 Emory Mouse Transgenic and Gene Targeting Core, Emory University School of Medicine, Atlanta, GA 30322, USA
7 Department of Pharmacology, Yong Loo Lin School of Medicine, National University of Singapore, Singapore 117600, Singapore
8 Emory Neurodegenerative Disease Center, Emory University School of Medicine, Atlanta, GA 30322, USA

†Present address: Department of Neurology, National Center for Neurological Disorders, Huashan Hospital, Shanghai Medical College, Fudan University, Shanghai 200040, China

‡Present address: Department of Neurology, Qilu Hospital of Shandong University, Jinan, Shandong 250012, China

Correspondence to: Hongjie Yuan
Department of Pharmacology and Chemical Biology, Emory University School of Medicine
1510 Clifton Road NE, Rollins Research Center, Atlanta, GA 30322, USA
E-mail: hyuan@emory.edu

Correspondence may also be addressed to: Hiro Furukawa
W.M. Keck Structural Biology Laboratory, Cold Spring Harbor Laboratory
1 Bungtown Road, New York, NY 11724, USA
E-mail: furukawa@cshl.edu

Keywords: NR2B; structural biology; seizure susceptibility; PET scan; translational study; precision medicine

Introduction

N-methyl-D-aspartate receptors (NMDARs) are ligand-gated cation-selective channels that bind to the neurotransmitter glutamate and mediate a slow, Ca^{2+}-permeable current at virtually all excitatory synapses in the CNS.[1] NMDARs are blocked by extracellular Mg^{2+} in a voltage-dependent manner,[2,3] which can be relieved by depolarization that, when paired with glutamate release, gives rise to an inward current. Voltage-dependent Mg^{2+} block enables NMDARs to act as coincidence detectors, which is important for multiple processes in the CNS, including learning, memory and neuronal development.[1] The *GRIN1*, *GRIN2A–GRIN2D* and *GRIN3A–GRIN3B* genes encode the GluN1, GluN2A–GluN2D and GluN3A–GluN3B NMDAR subunits. Combinations of two GluN1 and two GluN2 subunits or two GluN1 and two GluN3 subunits yield several distinct NMDAR assemblies, and potential mixing of GluN1, GluN2 and GluN3 subunits within a receptor complex can expand this diversity further.

NMDAR dysfunction is thought to be involved in neurological and neuropsychiatric disorders such as epilepsy, intellectual disability, autism spectrum disorder, neuropathic pain, depression, Parkinson's disease and schizophrenia.[1,4-7] In addition, an increasing number of rare *de novo* variants in *GRIN* genes (e.g. *GRIN1*, *GRIN2A*, *GRIN2B* and *GRIN2D*) have been identified by whole-exome sequencing in patients with various neurological and neuropsychiatric disorders.[8-18] Functional evaluation to determine how a disease-associated *GRIN* variant might influence receptor function is important to understand potential molecular mechanism underlying the phenotypes of patients. Functional analysis to evaluate multiple properties of *GRIN* variants has been performed in model systems.[12,18-23] We proposed an analytical and comprehensive framework to classify *GRIN* variants as either gain of function (GoF) or loss of function by integrating data from six different *in vitro* assays,[24] which is essential to evaluating variant pathogenicity, patient stratification and precision therapeutics, in addition to variant selection for making animal models.

NMDARs can be modulated by multiple exogenous compounds, many of which are subunit selective.[1,25] The pharmacology of GluN2B-selective negative allosteric modulators is well developed and includes a large number of scaffolds, several of which have progressed to clinical trials.[26-31] Among clinically relevant GluN2B-selective modulators, radiprodil is noteworthy for its potency and selectivity. Here, we explore the pharmacology and mechanism of action of radiprodil across NMDARs of varied GluN2 stoichiometry, define at atomic resolution its binding site, and show that radiprodil retains potency and efficacy for a number of different *GRIN1* and *GRIN2B* missense variants associated with various neurological and neuropsychiatric disorders. We demonstrate that radiprodil possesses antiseizure actions in a knock-in mouse model harbouring a gain-of-function GluN2B missense variant (*Grin2b*-S810R).

Materials and methods

Chemicals and solutions

All reagents and chemicals were obtained from Millipore Sigma (unless otherwise stated). Radiprodil was purchased from Cayman Chemical (Cat. No. 29712) and was aliquoted as powder. To generate a 1% methylcellulose solution, 1 g Methocel A15 LV (Sigma 64605-1006-F) was added gradually into 100 ml of 0.9% saline, heated to 40°C–45°C with magnetic stirring. The solution was clear after cooling to 4°C. To make 0.3 mg/ml stock solution, radiprodil was initially dissolved in DMSO (final 0.5% DMSO) and added under agitation to the 1% methylcellulose solution. A white, even suspension was formed when DMSO was combined with the drug and methylcellulose, which was injected intraperitoneally (i.p.). Vehicle was 0.5% DMSO in 1% methylcellulose in 0.9% saline. The mice were treated either with vehicle (VEH) or with radiprodil in vehicle (DRUG; 3 mg/kg weight, with volume of 10 ml/kg) by intraperitoneal injection 30 min before the tests. The 1% methylcellulose solution was kept at 4°C, and all other solutions were prepared freshly on the same day as the tests.

Molecular biology

Complementary DNAs encoding human GluN1-1a (GluN1, RefSeq NM_007327.3) and GluN2B (NM_000834.4) and rat GluN1-1a (NP_058706), GluN1-1b (NP_001257531.1), GluN2A (NP_036705),

GluN2B (NP_036706), GluN2C (NP_036707) and GluN2D (NP_073634) were subcloned into the pCI-neo plasmid, which was linearized with Not I and cRNA synthesized *in vitro* (mMessage machine, ThermoFisher Scientific). Triheteromeric NMDARs comprised rat GluN1 and GluN2A–GluN2D with modified C-terminal peptide tags as described previously[32-39] (Supplementary material, Methods). Patient-derived *GRIN1* and *GRIN2B* variants were introduced into human GluN1-1a and GluN2B cDNAs using the Quikchange protocol (Agilent). The full open reading frame was Sanger sequenced (Eurofins) to confirm that only the intended mutation was present.

Voltage-clamp recordings from *Xenopus laevis* oocytes

Stage V–VI *Xenopus laevis* oocytes were isolated as described,[24] and cRNAs (~10 ng total) were injected in a total volume of 50 nl to produce diheteromeric GluN1/GluN2A, GluN1/GluN2B, GluN1/GluN2C or GluN1/GluN2D or triheteromeric GluN1/GluN2A$_{C1}$/GluN2B$_{C2}$, GluN1/GluN2B$_{C1}$/GluN2C$_{C2}$ or GluN1/GluN2B$_{C1}$/GluN2D$_{C2}$ (Supplementary material, Methods). Two-electrode voltage-clamp current recordings were performed at room temperature as described.[33] Oocytes were perfused with (mM): 90 NaCl, 1 KCl, 10 HEPES and 0.5 $BaCl_2$; pH adjusted to 7.4 with 10 µM EDTA added to chelate trace divalent ions such as Zn^{2+}. The recording micropipettes were filled with 300 mM KCl (voltage electrode) or 3 M KCl (current electrode). The concentration–response relationship was determined by applying 100 µM glutamate and 30 µM glycine, followed by co-application of co-agonists with increasing concentrations of radiprodil. Radiprodil was applied for 3–6 min to achieve steady-state inhibition. Only oocytes with current responses of >50 nA were analysed. For all recordings on the triheteromeric recordings, the escape current attributed to diheteromeric receptors was <10% of the total current (Supplementary Fig. 1A). The current response amplitude was normalized to the response amplitude in the absence of radiprodil, and fitted by:

$$Present\ Response\ (\%) = (100 - minimum)/\{1 + ([radiprodil]/IC_{50})^{nH}\} + minimum \quad (1)$$

where IC_{50} is the concentration that produces half-maximal inhibition, minimum is the percentage response in saturating radiprodil, and n_H is the Hill slope.

Whole-cell patch-clamp recordings from HEK cells

Human embryonic kidney 293 cells (HEK; ATCC CRL-1573) were plated onto 0.1 mg/ml poly-D-lysine-pretreated glass coverslips in Dulbecco's modified Eagle medium (Gibco 10569-010, DMEM + GlutaMAX) supplemented with 10% dialysed fetal bovine serum, 10 U/ml penicillin, 10 µg/ml streptomycin, 200 µM DL-2-amino-5-phosphonopentanoic acid and 200 µM 7-chlorokynurenic acid. HEK cells were maintained at 37°C in a humidified environment with 5% CO_2 and transiently transfected with rat GluN1, GluN2B and enhanced green fluorescent protein cDNA (ratio 1:1:1, 0.5 µg per well[40]). Between 12 and 24 h post-transfection, coverslips were transferred to a recording chamber, and cells were perfused with recording solution containing (mM): 150 NaCl, 3 KCl, 0.01 EDTA, 1 $CaCl_2$, 10 HEPES and 22 D-mannitol (pH 7.4). Patch electrodes (3–5 MΩ) were made from thin-walled glass micropipettes (TW150F-4, World Precision Instruments) and contained (mM): 110 D-gluconate, 110 CsOH, 30 CsCl, 5 HEPES, 4 NaCl, 0.5 $CaCl_2$, 2 $MgCl_2$, 5 BAPTA, 2 NaATP and 0.3 NaGTP (pH adjusted to 7.4 with CsOH; 300–305 mOsmol/kg). Whole-cell currents in response to rapid application and removal of glutamate were recorded at a holding potential of −60 mV (23°C), low-pass filtered at 8 kHz (eight-pole Bessel, −3 dB) and digitized at 20 kHz. Responses >1 nA were corrected for series resistance filtering off-line.[41] The position of a two-barrelled theta-glass used for rapid solution exchange was controlled by a piezoelectric translator (Burleigh Instruments). The time course for onset and offset of radiprodil inhibition was fitted by:

$$Response = Amplitude[exp(-time/tau)] \quad (2)$$

The deactivation time course following rapid removal of glutamate was fitted by:

$$Response = Amplitude_{FAST}[exp(-time/tau_{FAST})] + Amplitude_{SLOW}[exp(-time/tau_{SLOW})] \quad (3)$$

The weighted deactivation tau (Tau_W, τ_W) was calculated by:

$$Tau_W = (Amplitude_{FAST}tau_{FAST} + Amplitude_{SLOW}tau_{SLOW})/(Amplitude_{FAST} + Amplitude_{SLOW}) \quad (4)$$

Voltage-clamp recording from acute hippocampal slices

Horizontal brain slices (280–300 µm thick) were prepared from wild-type (WT) C57BL/6J mice (Jackson Laboratory, postnatal Day 17–22) or knock-in mice (with their WT littermates as controls) from both sexes, as described in the Supplementary material, Methods. Slices containing hippocampus were transferred to a recording chamber and continuously perfused at a rate of 4 ml/min with oxygenated standard recording artificial CSF recording solution, which contained (mM): 126 NaCl, 26 $NaHCO_3$, 10 glucose, 2.5 KCl, 1.25 NaH_2PO_4, 1.5 $MgSO_4$ and 1.5 $CaCl_2$, bubbled with 95% O_2–5% CO_2. Neurons identified via infrared-differential interference contrast (DIC) optics, and voltage-clamp recordings were made using borosilicate micropipettes (1.5 mm outer diameter, 1.12 mm inner diameter; World Precision Instruments) pulled via a P-1000 micropipette puller (Sutter Instruments) and a Multiclamp 700B amplifier (Molecular Devices). Current recordings were filtered at 2 kHz using an eight-pole Bessel filter (−3 dB), digitized at 20 kHz using Axon pClamp10, and analysed off-line. The unpolished pipettes were filled with internal solution containing (mM): 105 caesium gluconate, 5 CsCl, 8 NaCl, 5 sodium phosphocreatine, 5 $MgCl_2$, 2 Na-ATP, 0.3 Na-GTP, 0.6 EGTA, 5 BAPTA, 40 HEPES and 5 QX314 (pH 7.3, adjusted with CsOH, ~290 mOsm). Pipette resistances were 4–7 MΩ. We added 10 µM gabazine and 10 µM NBQX to the external solution to block $GABA_A$ receptors and AMPA receptors, respectively. NMDA receptor-mediated excitatory postsynaptic currents (EPSCs) in cells held at +40 mV were evoked by injecting 50–120 µA of current for 0.1 ms using a monopolar platinum–iridium stimulating electrode (FHC) placed within the Schaffer collaterals in the stratum radiatum. The temperature was maintained at 30°C–32°C by an inline heater system (TC-344C, Warner Instruments). Series resistance was monitored continuously from the response to a −5 mV hyperpolarizing pulse applied prior to the synaptic stimuli, and analysed offline using the peak of the capacitive charging spike and Ohm's law. If the series resistance changed by >10% during the experiment, or exceeded 30 MΩ, the cell was excluded. Only stable

recordings were included, defined as those with a drift in series resistance of <10% over the course of the recordings.

Structural biology

Co-expression and purification of the *Xenopus* GluN1-1b and rat GluN2B N-terminal domain (NTD) heterodimer were described previously.[42,43] *Trichoplusia ni* (High Five, Thermo Fisher) insect cells were infected with a baculovirus harbouring *Xenopus* GluN1b NTD and rat GluN2B NTD cDNAs for 48 h. The concentrated medium was purified by Chelating-Sepharose charged with $CoCl_2$. Polyhistidine tags on the C-terminus of GluN1b NTD and the N-terminus of the GluN2B NTD were removed by thrombin digestion, and the samples were purified further by Superdex200 (GE Lifescience). Protein was concentrated to 10 mg/ml and dialysed against 50 mM NaCl, 10 mM Tris (pH 8.0) and 1 μM ifenprodil hemitartrate (Tocris). The dialysed protein was filtered through a 0.1 μm spin filter (Millipore) prior to the crystal screens. Crystals grew in sodium formate/HEPES,[42] taking 3–4 days to appear, then continuing to grow for 2–3 weeks at 18°C. Crystals were transferred to 2 μl drops containing 4 M sodium formate, 0.1 M HEPES (pH 7.5), 35 mM NaCl, 7 mM Tris (pH 8.0) and 50 μM radiprodil, and soaked overnight. Crystals were then transferred to a new drop of the same solution and soaked overnight again. Crystals were flash-frozen in liquid nitrogen for X-ray diffraction data collection by sequentially transferring them to 4.5 and 5 M sodium formate and leaving them overnight. Diffraction data were collected at the wavelength of 0.92 Å on the 17ID-1 beamline at the National Synchrotron Light Source II. Data were indexed and scaled by the software, XDS. The structure was solved by the molecular replacement method with the GluN1b–GluN2B ATD dimer in the PDB coordinate, 3QEL,[43] as a search probe using the program PHASER.[44] The structural model was refined by the program REFMAC, and the coordinate was modified by the program Coot.[45]

Grin2b-Ser810Arg mice

We used the CRISPR/Cas9 system to generate the *Grin2b* Ser810Arg (S810R) knock-in point mutation mouse line (Supplementary Fig. 2). One guide RNA (gRNA) and 180 bp Repair Donor were designed at the syntenic loci in the mouse genome. The Emory Mouse Transgenic and Gene Targeting core injected 20 ng/μl of gRNA, 20 ng/μl of Cas9 protein and 20 ng/μl of Repair Donor into single-cell C57BL/6J zygotes. Embryos were cultured overnight and transferred to pseudopregnant females. The resulting pups were screened for *Grin2b*-S810R mutation (AGC>AGG) via PCR. To confirm the desired mutation, Sanger sequencing was performed on purified PCR DNA from the potential mutant mice. Heterozygous mice progress to maturity; however, homozygous pups were not viable.

Mouse brain subcellular fractionation and immunoblotting

Adult (2- to 3-month-old) mouse whole brains were used for fractionation experiments as previously described.[46] Whole brain tissues were homogenized and lysates prepared as described in the Supplementary material, Methods. Ten micrograms of homogenate (Total) and 3 μg of postsynaptic density (PSD) proteins were used for immunoblotting. Antibodies were purchased as follows: rabbit anti-GluN2A (Abcam, Cat. No. ab124913), mouse anti-GluN2B (Neuromab, catalogue clone N59/36), rabbit anti-GluN1 (Abcam, Cat. No. 109182), rabbit anti-GluA1,[47] mouse anti-GluA2 (Neuromab, catalogue clone L21/32), mouse anti-PSD-95 (Neuromab, catalogue clone K28/43) and mouse anti-β-actin (abm, catalogue G043).

Golgi staining

For dendritic spine analysis, Golgi staining was performed in hippocampal slices with the FD Neurotech Golgi staining kit. For dendritic arborization, widefield z-stack images (z-spacing 1 μm) of impregnated CA1 pyramidal cells were obtained at ×20 and ×100 magnification. At least four dendrites from each mouse (four mice per condition) were imaged, and three-dimensional reconstructions were performed using NeuroLucida 360 to determine the number of spines per segment (normalized by length). Sholl analysis was used to determine the number of primary and secondary branch points. Spine density values were evaluated based on their distance from the soma, moving in 40 μm increments up to 240 μm. Spine geometry and size were evaluated. All analyses were performed blind.

Dynamic PET scans

Dynamic PET imaging was conducted for 60 min using a PET scanner (Molecubes). Adult *Grin2b*-S810R mice and their WT littermates were anaesthetized using isoflurane in medical oxygen and catheterized in the tail vein for intravenous bolus injection of tracers. Acquired PET data were reconstructed into 35 frames of increasing length (6 × 10 s, 8 × 30 s, 5 × 1 min, 10 × 2 min and 6 × 5 min). Image analysis was performed with PMOD v.4.2 software (PMOD Technologies). Time–activity curves (TACs) for the striatum, motor cortex, hippocampus, thalamus and cerebellum were extracted from dynamic PET images. Results are presented as the standard uptake value (SUV) calculated from the TACs.

Behavioural assays

Adult (8- to 30-week-old) *Grin2b*-S810R mice (C57BL/6J) and their WT littermates, with both sexes balanced, were acclimated to the behavioural room for ≥48 h prior to the beginning of the experiment. Food and water were available, and the room was on a standard 12 h–12 h light–dark cycle. Ear tags and toe clips were used to identify animals individually. Additional tail marking with different colours for short-term identification was performed immediately before the tests to minimize potential confounders. All procedures described were approved by the Institutional Animal Care and Use Committee at Emory University. A set of behavioural assays [rotarod, locomotor activity, Y-maze, novel object recognition (NOR), and elevated zero maze (EZM)] were performed as described in the Supplementary material, Methods. All animals in the behavioural assays were included in the analyses, except for mice with >15% body weight loss or severe skin wounds. To minimize observer bias, both the treatment groups during the behavioural assays and the data analyses were blinded to the experimenters and those performing analyses.

Determination of seizure threshold

Heterozygous knock-in *Grin2b*-S810R or WT littermate mice were assessed for response to intraperitoneal injection of pentylenetetrazole (PTZ; Sigma-Aldrich). The mouse was restrained by the scruff of the neck with the abdomen facing the operator and the head positioned slightly lower than the hindquarters, and a 27-gauge needle was inserted at a 45° angle through the skin and abdominal wall slightly to the left, lower quadrant. The PTZ solution (3.5–4.0 mg/ml) was prepared in sterilized saline (0.9% NaCl). We injected 10 ml/kg volume of material for a final dose of 35–40 mg/kg. At least eight mice per

genotype per condition were tested. Mice were observed and videotaped for 30 min immediately after injection, and the times to first myoclonic jerk, first generalized tonic–clonic seizure (GTCS), first GTCS plus bouncing, and hindlimb extension were recorded.

All *in vitro* studies were conducted according to the guidelines of Emory University and Cold Spring Harbor Laboratory. All animal work was performed according to the protocol of Emory University Institutional Care and Use Committee (IACUC).

Statistical analysis

Data are presented as the mean ± standard error of the mean (SEM) or the mean with the 95% confidence interval (CI), and the number of replicates is reported by *n*. Potency shifts for inhibitors and statistical comparisons (Student's two-tailed paired or unpaired *t*-test, Mann–Whitney U-test, or one-way ANOVA, with Bonferroni's multiple comparisons test) were performed in GraphPad Prism v.8.0.1 (La Jolla, CA, USA). The mean IC_{50} value and 95% CIs were calculated from the Log IC_{50} (half-maximal inhibitory concentration) values. The number of samples was calculated to produce a power to detect a 50% change of >0.8. Samples sizes were determined by *a priori* power analysis for effect size = 2, power = 0.8 and $\alpha = 0.05$. For analysis of the actions of radiprodil on *GRIN* variants, we evaluated the adjusted *P*-value from Student's unpaired *t*-test between variant and same-day control data using the Benjamini–Hochberg procedure to decrease type 1 errors, with a false discovery rate set to 0.01.

Results

Radiprodil potency at diheteromeric receptors containing two of the same GluN2 subunits

Radiprodil is a member of a class of piperadine-containing GluN2B antagonists.[48,49] We assessed the potency and subunit selectivity for radiprodil inhibition of NMDAR subtypes using two-electrode voltage-clamp recordings from *X. laevis* oocytes expressing recombinant NMDARs. We initially determined the IC_{50} value for radiprodil inhibition of diheteromeric rat and human NMDARs (Fig. 1A and C). Table 1 summarizes fitted IC_{50} values for radiprodil inhibition of the GluN1–GluN2B NMDAR responses to maximally effective concentrations of glutamate and glycine. Radiprodil was less potent on NMDARs that contained a GluN1 subunit that included residues encoded by the alternative exon 5 (GluN1-1b; Table 1). Given that the GluN1-1a isoform is the most extensively studied and well characterized, all further functional experiments were performed exclusively with the GluN1-1a isoform to ensure consistency and reduce experimental variability. Radiprodil was without effect on GluN2A, GluN2C and GluN2D diheteromeric receptors (Supplementary Fig. 1B). The application of saturating concentrations of radiprodil does not fully inhibit NMDARs. We therefore investigated the properties of the residual current following radiprodil binding. We found that radiprodil-bound (1 μM) diheteromeric NMDARs could be activated by glutamate with an EC_{50} value of 0.25 μM (Hill slope 0.82; $n = 7$ oocytes), compared with a control EC_{50} value of 1.1 μM (Hill slope 1.1; $n = 7$ oocytes) (Fig. 1E and F and Supplementary Table 1).

Radiprodil potency at triheteromeric receptors containing two different GluN2 subunits

NMDARs expressed *in vivo* in adulthood are often triheteromeric assemblies of two GluN1 subunits and two different GluN2 subunits. For example, at least half of the NMDARs in adult cortex and hippocampus are GluN1/GluN2A/GluN2B triheteromeric complexes,[50-55] which show some functional and pharmacological features that are distinct from diheteromeric receptors.[32,38,39,56,57] Additional studies support the concept of unique pharmacology and function of triheteromeric receptors with two different GluN2 subunits.[38,39] Han *et al.*[58] showed reduced inhibition of triheteromeric receptors by saturating concentrations of radiprodil, similar to what has been observed for other GluN2B antagonists.[59] We therefore examined in detail the actions of radiprodil on triheteromeric NMDARs that contain one copy of the GluN2B subunit using coiled-coil domains and an endoplasmic reticulum retention signal appended to the intracellular C-terminal to control subunit stoichiometry.[32] As expected, radiprodil was an effective inhibitor of the C-terminal-modified diheteromeric GluN2B receptors (GluN1/$GluN2B_{C1}$/$GluN2B_{C2}$) (Fig. 1B and D and Table 1) and retained inhibitory action at GluN2B-containing triheteromeric NMDARs, including GluN1/$GluN2A_{C1}$/$GluN2B_{C2}$, GluN1/$GluN2B_{C1}$/$GluN2C_{C2}$ and GluN1/$GluN2B_{C1}$/$GluN2D_{C2}$ (Table 1). However, the potency and extent of inhibition are reduced in triheteromeric assemblies compared with diheteromeric NMDARs that contain two copies of GluN2B. Interestingly, saturating concentrations of radiprodil produced stronger inhibition of triheteromeric receptors that contained GluN2C or GluN2D than GluN2A, similar to other GluN2-selective antagonists, such as CP101,606.[39]

Time course and agonist dependence of radiprodil

We evaluated the time course of radiprodil actions by rapidly applying different concentrations of radiprodil to NMDARs during the steady-state response to a maximally effective concentration of glutamate and glycine. We found a concentration-dependent association rate and progress into the inhibited state, consistent with the law of mass action governing the binding of radiprodil (Fig. 1G). The unbinding rate was impractical to measure because only a small amount of current was recovered (4.7% ± 1.2%) after 3 min of radiprodil washout (Fig. 1G). At this rate, it might take ≤1 h to recover fully from inhibition. Thus, using the intercept from the linear fit of the concentration-dependent association rate, we estimated a kinetically determined K_D of 0.175 μM (Fig. 1H). However, the unusually slow dissociation for radiprodil suggests that K_D should be lower.

Crystal structure of GluN1–GluN2B in complex with radiprodil

We explored the structural determinants of radiprodil binding at the heterodimer interface between the GluN1-1b (referred to as GluN1b for structural work on isolated NTD) and GluN2B amino terminal domains (NTDs) using X-ray crystallography. We solved the structure of the isolated GluN1b–GluN2B NTD heterodimer in complex with radiprodil at 2.74 Å resolution (Fig. 2 and Supplementary Table 2). Here, the GluN1-1b splice variant was used because well-diffracting crystals could not be obtained for the GluN1-1a isoform. The GluN1b–GluN2B NTD structure is nearly identical to that of the GluN1a–GluN2B NTD dimer in the intact GluN1a–GluN2B NMDARs, apart from differences around the exon 5-encoded region,[60] which does not contribute directly to radiprodil binding. Therefore, the overall structural insights derived from the GluN1b–GluN2B NTD can be directly applicable to the GluN1a–GluN2B NMDAR. The GluN1 and GluN2B NTDs have bi-lobe architectures composed of the upper (R1) and lower (R2) domains (Fig. 2B). Radiprodil binds at the GluN1b–GluN2B subunit interface, thus, there are two radiprodil binding sites within the intact tetramers. The structure of

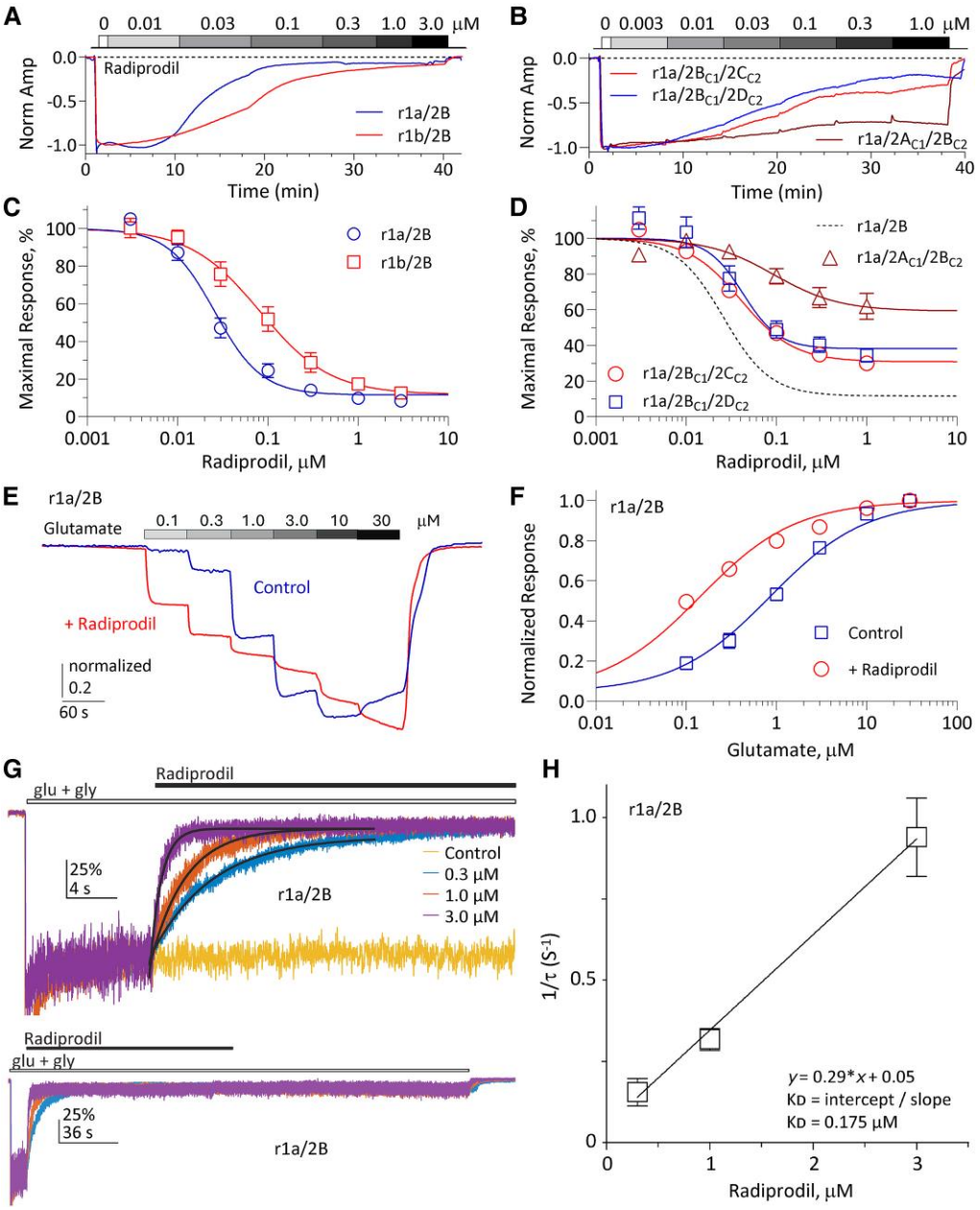

Figure 1 Inhibition of diheteromeric and triheteromeric NMDA receptors by the GluN2B-selective compound radiprodil. (**A** and **C**) Di-heteromeric rat GluN2B-containing NMDARs expressed with different N-terminal GluN1 splice variants (1a or 1b, as indicated). (**A**) Representative normalized current responses recorded from *Xenopus* oocytes using two-electrode voltage clamp show the concentration–response relationship for radiprodil inhibition of rat GluN2B NMDARs expressed with either GluN1-1a (lacking exon 5) or GluN1-1b (including exon 5). Current responses were activated by saturated concentrations of glutamate (Glu, 100 μM) and glycine (Gly, 30 μM), applied as indicated by the white box; increasing concentrations of radiprodil are shown by greyscale boxes (0.01, 0.03, 0.1, 0.3, 1 and 3 μM, as indicated). (**B**) Representative current responses for radiprodil inhibition of rat triheteromeric NMDARs activated by saturated concentrations of glutamate (100 μM) and glycine (30 μM) are shown (white box), with increasing concentrations of radiprodil indicated by the greyscale boxes (0.003, 0.01, 0.03, 0.1, 0.3 and 1 μM). (**C**) The concentration–response relationships for radiprodil inhibition of rat diheteromeric NMDARs containing two GluN1 splice variants are shown. (**D**) The concentration–response relationships for radiprodil inhibition of triheteromeric NMDAR-mediated current responses for GluN1/GluN2A$_{C1}$/GluN2B$_{C2}$, GluN1/GluN2B$_{C1}$/GluN2C$_{C2}$ and GluN1/GluN2B$_{C1}$/GluN2D$_{C2}$ are shown. All triheteromeric subunit combinations were expressed with the GluN1-1a splice variant. The fitted diheteromeric GluN1-1a/GluN2B trace from **C** is superimposed as a dotted line for comparison. (**E**) Representative current responses recorded from *Xenopus* oocytes show the concentration–response relationship for glutamate activation of rat GluN2B NMDARs expressed with GluN1-1a in the absence or presence of 1 μM radiprodil. (**F**) Concentration–response relationship for glutamate in the absence and presence of radiprodil (present in wash and agonist solutions). (**G** and **H**) The time course for the onset of radiprodil inhibition. (**G**) *Top*: Concentration-dependent binding of radiprodil to rat GluN1/GluN2B NMDARs was assessed in HEK293 cells recorded under voltage clamp. The steady-state level of inhibition for all radiprodil concentrations approached that observed for saturating concentrations of antagonists (0.3 μM, 6.0% of control; 1 μM, 7.9% of control; 3 μM, 6.7% of control). *Bottom*: Radiprodil washout proceeds very slowly, with a 3-min washout producing negligible recovery from inhibition (4.7% recovery from inhibition, which suggests a 62 min recovery tau, assuming an exponential time course). (**H**) A single exponential function could describe the relaxation during radiprodil application. The association and dissociation rates were determined from the linear relationship between radiprodil concentration and the reciprocal of the fitted deactivation tau, consistent with the law of mass action. The kinetically determined K_D (dissociation constant) was approximated to be 0.175 μM by the ratio of the fitted linear intercept (k_{off}, dissociation rate constant) and the slope (k_{on}, association rate constant). Data were expressed as the mean ± standard error of the mean.

Table 1 Inhibition of NMDA receptor function by radiprodil

Receptor	IC_{50}, μM, mean [95% CI]	*n*H, mean ± SEM	Maximum inhibition, %, mean ± SEM	*n*
Human GluN1-1a/GluN2B	0.029 [0.023, 0.035]	1.4 ± 0.1	91 ± 1.0	13
Rat GluN1-1a/GluN2B	0.026 [0.0085, 0.038]	1.7 ± 0.3	82 ± 9	16
Rat GluN1-1b/GluN2B	0.13 [0.081, 0.17]	1.9 ± 0.1	83 ± 3	19
Rat GluN1-1a/GluN2A_{C1}/GluN2B_{C2}	0.091 [0.047, 0.13]	1.4 ± 0.3	45 ± 10	8
Rat GluN1-1a/GluN2B_{C1}/GluN2C_{C2}	0.035 [0.026, 0.041]	1.7 ± 0.1	64 ± 5	13
Rat GluN1-1a/GluN2B_{C1}/GluN2D_{C2}	0.054 [0.021, 0.059]	1.4 ± 0.3	65 ± 4	16

Radiprodil concentration–inhibition results for *N*-methyl-D-aspartate receptors (NMDARs) expressed in *Xenopus* oocytes and activated by 100 μM glutamate and 30 μM glycine. The Hill equation was fitted to responses from each oocyte, and the mean with 95% confidence interval (CI) calculated from the log(IC_{50}), or mean ± standard error of the mean (SEM). *n* is the number of oocytes evaluated. EC_{50} = half maximal effective concentration; IC_{50} = half-maximal inhibitory concentration; *n*H = Hill slope.

the isolated NTDs is similar to the NTDs of the intact tetrameric receptors [root mean square deviation (RMSD) = 0.595 Å over 590 Cα positions between the A/B chain of the GluN1a–GluN2B NTD crystal structure and the structure with the 4PE5 PDB code]. Therefore, the radiprodil-bound structure presented here is physiologically relevant and serves as an excellent model for understanding the binding mode (Fig. 2B–D).[42,43,61,62] Radiprodil was localized to the same binding pocket as ifenprodil, EU93-31 and other previously published biaryl GluN2B-selective negative allosteric modulators (NAMs)[61,63] (Fig. 2E and F). With respect to overall conformations, the GluN1b–GluN2B NTD–radiprodil structure is highly similar to the ifenprodil-bound conformation of the intact GluN1b-2B NMDAR (RMSD versus 4PE5 = 0.595 Å over 590 Cα positions).[61] It is more similar to the non-active conformation of the agonist-bound intact GluN1b-2B NMDARs (RMSD versus 7SAA = 1.806 Å over 660 Cα carbons; Supplementary Fig. 3), where the bi-lobe structure (composed of R1 and R2) of GluN2B NTD is closed,[61,64-66] than to the active conformation, in which the GluN2B NTD bi-lobes are open.[64,66]

The quality of the electron density is sufficient for identification and modelling of the radiprodil molecule (Fig. 2), which permits visualization of the binding mode (Fig. 2). The structural data showed that residues from GluN1b and GluN2B NTDs, especially around the α3 helix from GluN1b and α2′ and α6′ from GluN2B, were in contact with radiprodil. The 2-oxo-benzoxazol group of radiprodil forms polar interactions with the backbone amides of GluN2B-Met207 and the GluN2B-Glu236 side chain from α6′ in the R2 lobe. Radiprodil has more extensive polar interactions than ifenprodil,[43] involving both GluN2B-Met207 and GluN2B-Glu236 (Fig. 2E). EU93-31 has the same set of polar interactions as radiprodil, but involving the sulfonamide group instead of the 2-oxobenzoxazol group (Fig. 2F). The fluorophenyl group and the piperadine ring are in van der Waals contacts with multiple residues, including GluN2B-Pro78, -Phe176, -Pro177, -Ile111 and -Phe114 and GluN1b-Phe113, -Ile133 and -Leu135, located mainly in the R1 lobe (Fig. 2D). The van der Waals contacts are similar between radiprodil and ifenprodil (Fig. 2E) but distinct from the EU93-91 owing to their differences in the backbone configurations (Fig. 2F, arrow). Overall, the compound binding involves hydrophobic interactions with the R1-lobe residues and polar interactions with the R2-lobe residues. Consequently, the GluN2B NTD bi-lobes would close, and GluN1–GluN2B NTD dimer interfaces rearrange and stabilize the inhibited state.[64,66] The strength of these van der Waal and polar interactions would, therefore, control the stability of the inhibited conformation and the channel inhibition.

Radiprodil potency at NMDARs harbouring human variants

The *GRIN* gene family is intolerant to variation, and a large number of missense variants that are absent from the general population have been observed in patients with neurological conditions. Many of these variants can enhance receptor function, often referred to as a GoF.[18,58,67] Prior studies showed that the GluN2B allosteric antagonist radiprodil, which can reduce seizure burden in patients with infantile spasms,[29] inhibits diheteromeric GluN2B receptors harbouring two copies of rare GluN2B *de novo* GoF variants,[68] in addition to triheteromeric receptors with one copy of GluN2A and one copy of variant GluN2B.[58] We sought to determine further whether variants in different regions of the NMDAR retained sensitivity to radiprodil, which might indicate that radiprodil could mitigate some aspects of GluN2B-containing NMDAR overactivation. We evaluated 27 GoF *GRIN1* and *GRIN2B* variants in the NTD, the agonist-binding domain (ABD), the transmembrane domains (TMDs) and the linker regions connecting these domains.[1,18,22,69-72] Variants localized in different subdomains can drive unique electrophysiological effects by distinct mechanisms, and thus neurological phenotypes in patients can vary.[12,13,16,18]

We recorded the concentration–response relationship for radiprodil inhibition of WT and five variant GluN1- and 22 variant GluN2B-containing NMDARs. Table 2 summarizes the results of the analysis of variant NMDARs. These data show strong inhibition produced by radiprodil in most of the 27 GluN1 and GluN2B variants tested. We found five GluN2B variants that showed a significant reduction in potency, as demonstrated by these increases in IC_{50} values: A639V 23-fold, I655F 4.5-fold, A652G 3.2-fold, M818T 2.8-fold and S810R 1.9-fold. We also found that five GluN2B variants had significantly less (2.0- to 4.4-fold) maximal overall inhibition (I150V, A639V, A652G, I655F and M818T), determined from the magnitude of the fitted residual current response in a saturating concentration of radiprodil (Table 2). Five GluN2B variants exhibited a modest 1.4- to 1.6-fold increase in radiprodil potency (N616I, N616S, W607S, G611V and E657G). None of the GluN1 variants tested showed an altered response to radiprodil. These data support the idea that radiprodil is equally or more effective than WT receptors in 81% (22/27) of variant NMDARs tested. These data also suggest that radiprodil is capable of inhibiting GoF variants located in multiple regions, including the amino terminal domain, agonist-binding domain, pore-forming region and the linkers.

The missense variant GluN2B-Ser810Arg produces a likely gain of function

To evaluate further the effect of radiprodil on GoF *GRIN* variants, we studied the variant GluN2B-S810R, which resides in the pre-M4 linker region (Fig. 3A and B) and has previously been identified in a patient with intellectual disability, focal seizures, malformation of cortical development, and microcephaly.[67] The initial functional characterization[67] revealed increased co-agonist potencies, with no change in Mg^{2+} sensitivity. We have repeated these experiments

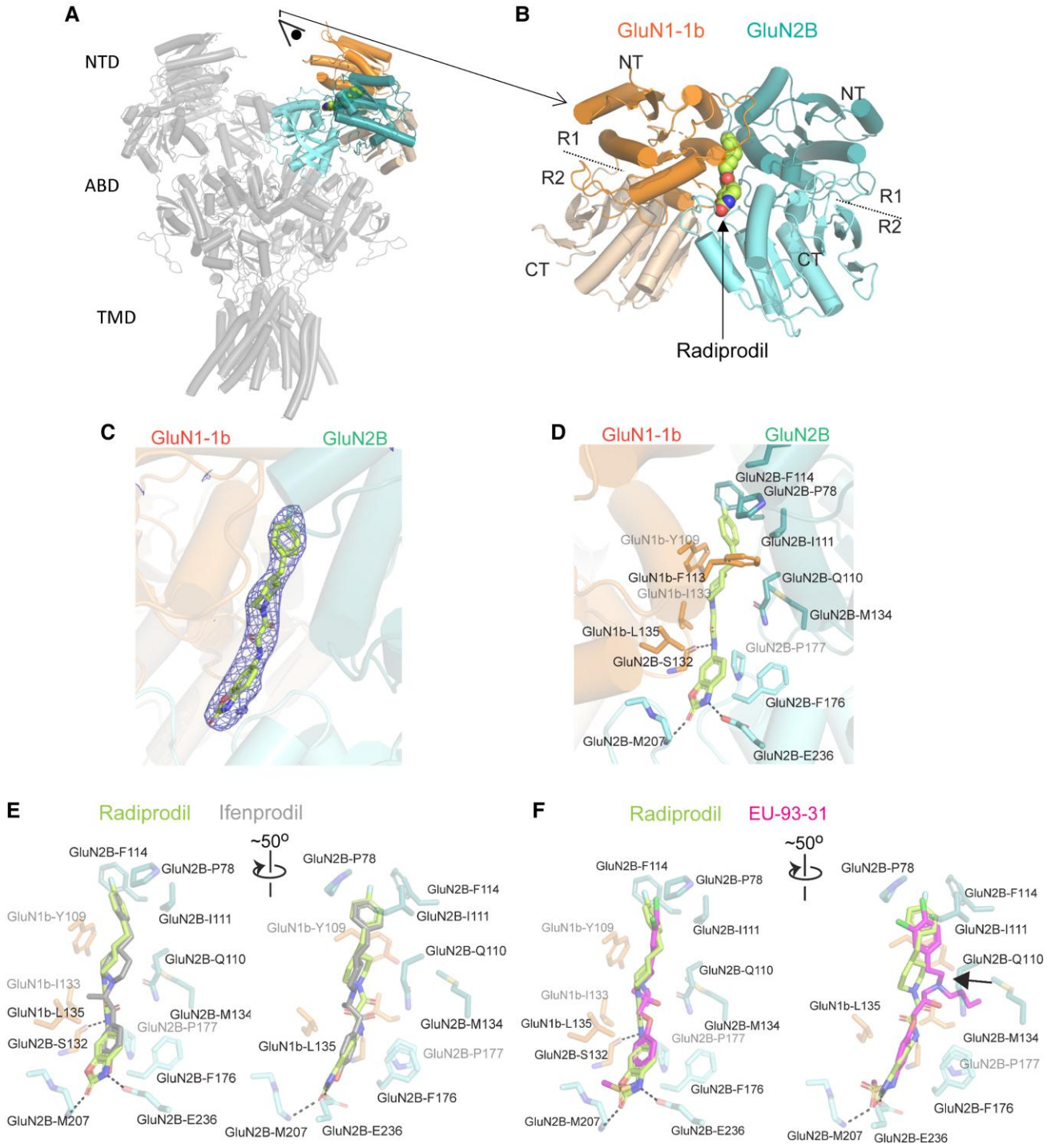

Figure 2 Structure of GluN1-1b–GluN2B NTD in complex with radiprodil. (**A**) The GluN1b–GluN2B NTD (N-terminal domain) bound to radiprodil (spheres) is superimposed on the structure of the intact GluN1–GluN2B NMDAR in complex with glycine and glutamate (PDB code: 7SAA). (**B**) GluN1-1b–GluN2B NTD viewed from the eye in **A**. The upper and lower lobes are annotated as R1 and R2, respectively. (**C**) The *Fo-Fc* omit map of the radiprodil density contoured at 4.5σ (mesh) and the modelled radiprodil (sticks). (**D**) Binding of radiprodil at the dimer interface between GluN1-1b and GluN2B. (**E** and **F**) Comparison of binding poses between radiprodil and ifenprodil (**E**) or EU93-31 (**F**). The GluN1-1b subunits of the ifenprodil-bound or EU93-31-bound structures were superimposed onto the radiprodil-bound structure. An arrow in **F** indicates the large difference in the binding mode between radiprodil and EU93-31.

and completed new assays that are necessary for a determination of gain or loss of function, as described by Myers *et al.*[24] We confirmed the increase in glutamate and glycine potency, in addition to a reduction in tonic proton inhibition at physiological pH (Fig. 3C, D and F). We also confirmed no effect of this variant on the IC_{50} value for extracellular Mg^{2+} inhibition (Fig. 3E). We recorded the time course of NMDAR-mediated currents from transfected HEK cells in response to rapid agonist application and found that

Table 2 Inhibition of NMDA receptor *GRIN* variant function by radiprodil

GRIN variants	PMID or ClinVar	Domain	Mutant/WT synaptic charge transfer	Mutant/WT non-synaptic charge transfer	IC_{50}, inhibition %, (*n*)
WT GluN1/GluN2B	–	–	1.0	1.0	35 nM, 85%, (253)
GluN2B-I150V	PMID 37369021	NTD	1.1	1.7	33 nM, 31%*, (10)
GluN2B-P259H	RCV002926524	NTD	1.3	2.9	48 nM, 89%, (10)
GluN2B-S541G	PMID 37369021	S1-M1	1.8	4.4	44 nM, 80%, (10)
GluN2B-W607S	PMID 37369021	M2	7.1	7.2	20 nM*, 87%, (5)
GluN2B-G611V	PMID 373690211	M2	28	12	24 nM*, 85%, (10)
GluN2B-N616I	PMID 38766179	M2	89	173	25 nM*, 88%, (11)
GluN2B-N616S	PMID 38766179	M2	12	9.3	22 nM*, 88%, (10)
GluN2B-V620M	PMID 37369021	M2	8.6	9.9	37 nM, 77%, (10)
GluN2B-A639V	PMID 38538865	M3	7.9	6.2	1041 nM*, 37%*, (6)
GluN2B-A652G	PMID 38538865	M3	6.3	12	113 nM*, 71%*, (7)
GluN2B-M654I	PMID 38766179	M3	5.9	8.4	50 nM, 88%, (10)
GluN2B-M654V	PMID 38766179	M3	2.0	14	65 nM, 84%, (10)
GluN2B-I655F	PMID 38538865	M3	1.5	2.0	181 nM*, 66%*, (9)
GluN2B-E657G	VCV000234479.3	M3-S2	0.041	3.7	21 nM*, 82%, (8)
GluN2B-E657D	PMID 37369021	M3-S2	1.7	2.4	23 nM, 85%, (10)
GluN2B-R682C	VCV000029730.6	ABD (S2)	NA	NA	33 nM, 84%, (10)
GluN2B-R682H	PMID 37369021	ABD (S2)	3.2	3.9	36 nM, 87%, (11)
GluN2B-R693S	PMID 37369021	ABD (S2)	5.1	10	43 nM, 88%, (10)
GluN2B-R696C	PMID 38766179	ABD (S2)	3.0	12	29 nM, 86%, (9)
GluN2B-R696H	PMID 37369021	ABD (S2)	1.5	4.8	36 nM, 85%, (10)
GluN2B-S810R	This study	S2-M4	21	57	53 nM*, 89%, (12)
GluN2B-M818T	PMID 38766179	M4	2.6	5.4	79 nM*, 81%*, (13)
GluN1-Q556R	PMID 39535073	ABD (S1)	15	25	32 nM, 84%, (4)
GluN1-A637S	PMID 38538865	M3	3.4	2.0	17 nM, 87%, (7)
GluN1-M641L	PMID 38538865	M3	4.0	11	38 nM, 85%, (7)
GluN1-E737K	VCV003544383.1	ABD (S2)	0.74	0.69	25 nM, 88%, (6)
GluN1-A806E	PMID 39535073	pre-M4	8.7	14	12 nM, 84%, (4)

Radiprodil concentration–effect curves were recorded under two-electrode voltage clamp from human *N*-methyl-D-aspartate receptors (NMDARs) expressed in oocytes. The individual concentration–response curves were fitted by the Hill equation (see the 'Materials and methods' section), and the mean IC_{50} value and percentage maximal inhibition at saturating radiprodil concentration are reported. The relative synaptic and non-synaptic charge transfer were calculated as described by Myers *et al.*[24] and were obtained from published data; data for variants not previously published are in Supplementary Table 3. NA indicates data not available because responses in some assays (Tau determination in HEK cells, open probability) were too small to measure. Mean wild-type (WT) IC_{50} was calculated from same-day control recordings pooled from all experiments. ABD = agonist binding domain; EC_{50} = half maximal effective concentration; IC_{50} = half-maximal inhibitory concentration; NTD = N-terminal domain.
*$P < 0.05$ for Log IC_{50} or mean residual current obtained from fits to each concentration–response curve for each oocyte by Student's unpaired *t*-test compared with same-day controls. We used Benjamini–Hochberg correction for false discovery rate (set to 0.01).

this variant prolongs the time constant describing deactivation (Fig. 3G and H). We also showed that the variant increased open probability without markedly changing the surface expression relative to WT NMDARs (Fig. 3I and J). These results show that the GluN2B-S810R variant enhances receptor-mediated charge transfer in multiple conditions and can be classified as likely GoF, with predicted relative increases in synaptic and non-synaptic charge transfer of 21- and 57-fold (Table 3), respectively.[24]

Effects of radiprodil on mutant mice harbouring GluN2B-Ser810Arg

We developed a knock-in mouse line (Supplementary Fig. 2) that harboured the single nucleotide change (c.2430C>A) giving rise to the GoF GluN2B-S810R variant. We studied this mouse line to elucidate the *in vivo* consequences of this variant by using a series of electrophysiological, anatomical, metabolic and behavioural assays. We also evaluated the ability of radiprodil to mitigate the circuit and/or behavioural alternations caused by the variant. The heterozygous GluN2B-S810R mice showed a tendency towards reduced body weight (Supplementary Fig. 4), raising the possibility that this variant alters development. We initially evaluated whether the GluN2B-S810R variant influences the expression of NMDAR subunits, AMPAR subunits and membrane-associated guanylate kinase (MAGUK) proteins. To investigate their expression in total homogenate and in synaptic fractions, we performed the subcellular fractionation assay using adult WT and GluN2B-S810R heterozygous mouse whole brain. The protein expression of NMDAR subunits (GluN2A, GluN2B and GluN1) and AMPAR subunits (GluA1 and GluA2), in addition to the MAGUK protein PSD-95, in both total and PSD fractions were not significantly different (Fig. 3K–N and Supplementary Fig. 5).

We assessed how the GluN2B-S810R variant influenced synaptic connectivity and activity. Stimulation of the Schaffer collaterals during whole-cell voltage-clamp recordings of hippocampal CA1 pyramidal neurons from brain slices allowed us to record evoked excitatory postsynaptic currents (eEPSCs). Knock-in mice that contained GluN2B-S810R showed an enhanced NMDAR EPSC amplitude at lower stimulus intensities (Fig. 4A–D and Table 3). We subsequently performed Golgi staining on four WT and four heterozygous GluN2B-S810R mice and assessed the number and morphology of dendritic spines. Analysis of dendritic spines in hippocampal CA1 pyramidal cells revealed a significant decrease in spine density in mice harbouring the GluN2B-S810R variant (Table 3 and Fig. 4E and F). This was manifested primarily as a loss of larger mushroom-shaped spines (Fig. 4F) that are often considered mature. We then performed *in vivo* dynamic PET scans to evaluate the influence of the GluN2B-S810R variant on cerebral

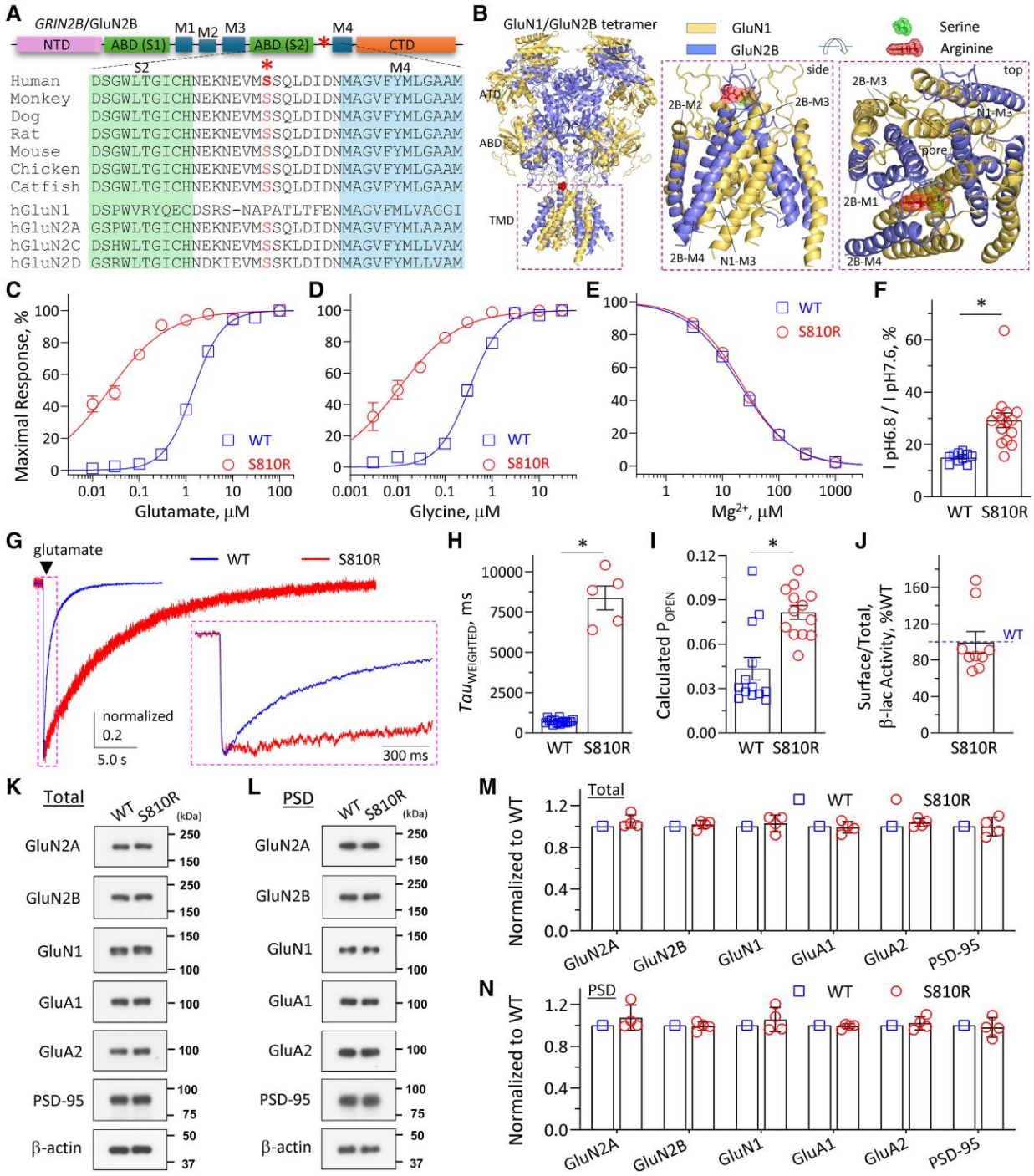

Figure 3 The missense variant GluN2B-S810R produces a likely gain of function and unchanged expression of synaptic proteins in GluN2B-S810R heterozygous mouse brain. (**A**) Linear schematic diagram of a cDNA encoding different NMDAR domains, with the pre-M4 linker expanded below. Ser810 is conserved across species and within the GluN2 gene family. (**B**) The substitution of Arg for Ser at position 810 produces steric and electronic changes to the protein at a site that is critically involved in gating.[72] (**C** and **D**) Concentration–response curves show an increase in potency of GluN2B-S810R for glutamate (**C**; variant EC_{50} 0.023 μM, WT EC_{50} 1.4 μM, $n = 13$ or 14) and glycine (**D**; variant EC_{50} 0.0064 μM, WT EC_{50} 0.32 μM) compared with WT controls recorded on the same day. (**E**) There was no detectable effect on the potency of Mg^{2+} inhibition evaluated at −60 mV (variant IC_{50} 20 μM, WT IC_{50} 22 μM, $n = 12$–19). (**F**) There was a clear reduction in proton sensitivity, with the ratio of current recorded at pH 6.8 to pH 7.6 for variant being 29% ± 2.8% ($n = 15$) and for WT being 15% ± 0.60% ($n = 10$). (**G** and **H**) The weighted mean time constant ($Tau_{WEIGHTED}$) describing the time course for deactivation following rapid removal of glutamate was prolonged from 708 ± 33 ms ($n = 17$) to 8370 ± 745 ms ($n = 5$) for the variant. (**I**) The open probability was increased for the variant (0.082 ± 0.0046, $n = 13$) compared with WT (0.043 ± 0.0076, $n = 13$). (**J**) There was no detectable change in the surface expression relative to WT controls (100% ± 12%, $n = 9$ experiments). (**K**–**N**) Using adult WT and GluN2B-S810R heterozygous mouse whole brain, a subcellular fractionation assay was performed as described in the 'Materials and methods' section, and homogenates (Total) and PSD lysates were immunoblotted with indicated antibodies. (**M** and **N**) Quantification of blots divided by β-actin, then normalized to WT ($n = 4$ independent experiments). Each band intensity in homogenate (Total) using GluN2A ($P = 0.0955$), GluN2B ($P = 0.2017$), GluN1 ($P = 0.2544$), GluA1 ($P = 0.3796$), GluA2 ($P = 0.0581$) and PSD-95 ($P = 0.4787$), in addition to GluN2A ($P = 0.1368$), GluN2B ($P = 0.3667$), GluN1 ($P = 0.1865$), GluA1 ($P = 0.2895$), GluA2 ($P = 0.2615$) and PSD-95 ($P = 0.3550$) in the PSD fraction, was measured using ImageJ software (NIH). Error bars represent ± standard error of the mean. Student's unpaired *t*-test, $^*P < 0.05$. EC_{50} = half maximal effective concentration; IC_{50} = half-maximal inhibitory concentration; PSD = postsynaptic density; WT = wild-type.

Table 3 Properties of GluN2B-S810R variant and heterozygous GluN2B-S810R mice

Parameters	Wild-type	GluN2B-S810R
Oocytes, HEK cells		
Glutamate EC_{50}, μM	1.4 [1.2, 1.6] (13)	0.023 [0.013, 0.042] (14)[a]
Glycine EC_{50}, μM	0.32 [0.27, 0.38] (10)	0.0064 [0.0026, 0.016] (13)[a]
%, pH 6.8/pH 7.6	15 ± 0.6 (10)	29 ± 2.8 (15)*
Mg^{2+} IC_{50}, μM	20 [17, 24] (19)	22 [19, 27] (12)
$Tau_{weighted}$, ms	708 ± 33 (17)	8370 ± 745 (5)*
P_{OPEN}, MTSEA	0.043 ± 0.0076 (13)	0.082 ± 0.0046 (13)*
Surface/total ratio (beta-lac)	1.0 (7)	1.1 ± 0.36 (5)
Synaptic charge transfer	1.0	21
Non-synaptic charge transfer	1.0	57
Slices		
eEPSC amplitude, pA	43 ± 2.0 (12)	52 ± 1.7 (17)
Normalized eEPSC amplitude, pA	55 ± 4.6 (12)	121 ± 3.5 (17)*
Decay time, ms	107 ± 79 (12)	74 ± 38 (17)
Total spine, number/mm	0.99 ± 0.02 (4)	0.54 ± 0.01 (4)*
Thin spine, number/mm	0.38 ± 0.02 (4)	0.17 ± 0.01 (4)*
Mushroom spine, number/mm	0.39 ± 0.04 (4)	0.29 ± 0.02 (4)
Stubby spine, number/mm	0.21 ± 0.01 (4)	0.10 ± 0.01 (4)*
PET scan, FDG		
Whole brain	1.19 ± 0.049 (5)	0.88 ± 0.048 (8)*
Cortex	1.20 ± 0.049 (5)	0.88 ± 0.050 (8)*
Hippocampus	1.24 ± 0.042 (5)	0.92 ± 0.052 (8)*
Thalamus	1.23 ± 0.053 (5)	0.89 ± 0.050 (8)*
Striatum	1.21 ± 0.082 (5)	0.88 ± 0.048 (8)*
Cerebellum	1.18 ± 0.046 (5)	0.93 ± 0.052 (8)*
Animals		
Rotarod: latency, s	115 ± 6.6 (17)	106 ± 5.2 (31)
Locomotor: total distance, mm	6043 ± 341 (16)	5411 ± 352 (32)
Y-maze: % correct alternation	66 ± 2.3% (12)	64 ± 1.7% (12)
Y-maze: arm entries	44 ± 3.3 (12)	56 ± 3.2 (12)*
NOR: novelty preference, %	69 ± 6.1% (12)	54 ± 7.3% (12)
NOR: travel distance (Day 1), mm	24,204 ± 1469 (12)	30,803 ± 1568 (12)*
EZM: number of open arm crossings	7.1 ± 1.7 (16)	4.1 ± 1.1 (30)
EZM: time in open arm, s	47 ± 7.9 (16)	33 ± 7.5 (30)
Delay to PTZ: induced myoclonic jerk, s	115 ± 4.4 (10)	58 ± 1.6 (10)*
Delay to PTZ: induced GTCS, s	309 ± 18 (5)	183 ± 7.2 (10)*
Animals undergoing GTCS	5/10	10/10
Rescue: slices		
Vehicle: eEPSC amplitude, pA	33 ± 5.6 (6)	48 ± 11 (9)
Radiprodil: eEPSC amplitude, pA	16 ± 2.3 (6)#	25 ± 5.9 (9)#
Vehicle: eEPSC decay, ms	122 ± 46 (6)	80 ± 14 (9)
Radiprodil: eEPSC decay, ms	82 ± 11 (6)	61 ± 7.2 (9)
Rescue: animals		
Vehicle: delay to PTZ-induced myoclonic jerk, s	175 ± 39 (19)	99 ± 8.4 (20)
Radiprodil: delay to PTZ-induced myoclonic jerk, s	244 ± 65 (17)	131 ± 33 (26)
Vehicle: delay to PTZ-induced GTCS, s	352 ± 58 (5)	207 ± 23 (20)
Radiprodil: delay to PTZ-induced GTCS, s	502 ± 70 (6)	458 ± 90 (16)#
Vehicle: animals undergoing GTCS (%)	5/21 (24%)	20/21 (95%)
Radiprodil: animals undergoing GTCS (%)	6/18 (33%)	16/26 (62%)

Data are presented as mean [95% confidence interval] calculated from the log(EC_{50}) and log(IC_{50}), or mean ± standard error of the mean. For spine analysis, we evaluated the three-dimensional collapse to a projection image for branches in 16 cells from four different animals per condition. EC_{50} = half maximal effective concentration; eEPSC = evoked excitatory postsynaptic current; EZM = elevated zero maze; FDG = fluorodeoxyglucose; GTCS = generalized tonic–clonic seizures; IC_{50} = half-maximal inhibitory concentration; NOR = novel object recognition; PSD = postsynaptic density; PTZ = pentylenetetrazole.

[a]Ninety-five per cent confidence intervals (CIs) that are non-overlapping with wild-type GluN1/GluN2B-containing *N*-methyl-D-as partate receptors (NMDARs).

*$P < 0.05$, Student's unpaired *t*-test, compared with wild-type.

#$P < 0.05$, Student's unpaired *t*-test, compared with the vehicle/control group of the same genotype.

glucose metabolism. We used ^{18}F-fluorodeoxyglucose (^{18}F-FDG) to measure cerebral rates of glucose metabolism quantitatively. Our data indicate that the adult heterozygous S810R mice present a reduced glucose metabolism in the whole-brain level, in addition to several specific brain regions, such as cortex, hippocampus, thalamus, striatum and cerebellum (Fig. 4G and H and Table 3).

We performed a series of baseline behavioural tests (rotarod, locomotor, novel object recognition, Y-maze and elevated zero maze) on WT and GluN2B-S810R mice to assess coordination, motor function, exploratory behaviour, learning/memory and anxiety. Table 3 and Fig. 4I–L summarize the results of these tests, which show no marked differences in the latency to falling (rotarod),

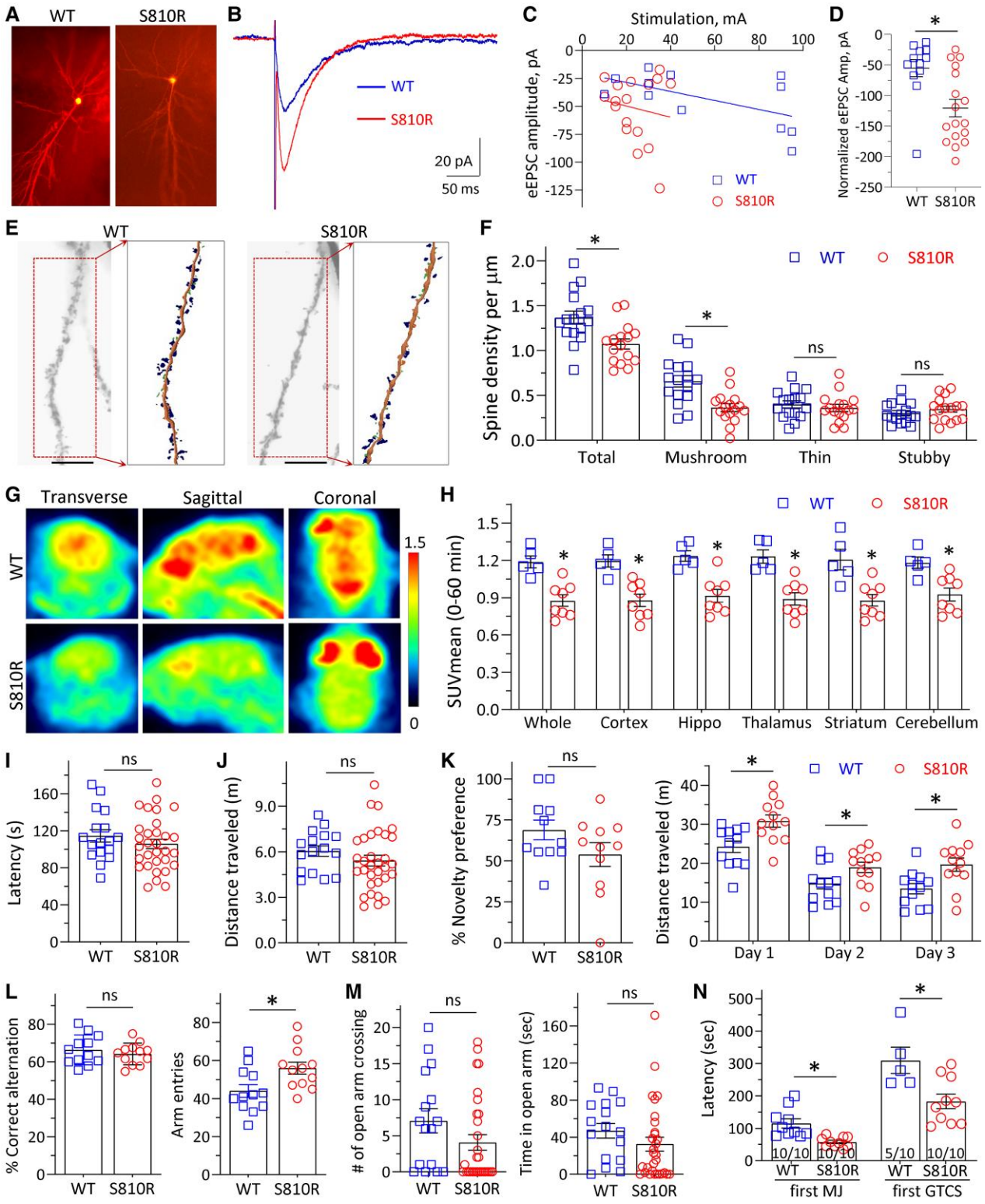

Figure 4 Effects of GluN2B-S810R on NMDAR-mediated EPSCs, dendritic spine density, cerebral glucose metabolism, behaviours and seizure threshold. (**A**) Representative CA1 pyramidal cells that were filled with dye during patch-clamp recording. (**B**) Representative evoked NMDAR-mediated EPSCs were recorded in CA1 pyramidal cells in response to Schaffer collateral stimulation in the presence of the AMPA receptor antagonist NBQX and reduced extracellular Mg^{2+} (0.2 mM). (**C**) Input–output curve for stimulus intensity versus the amplitude of the evoked NMDAR-mediated component of the EPSC (eEPSC) in CA1 pyramidal cells recorded from WT and GluN2B-S810R hippocampal slices. (**D**) Evoked NMDAR-mediated EPSC amplitude for WT and GluN2B-S810R CA1 pyramidal cells. (**E** and **F**) Dendritic spines in CA1 pyramidal cell by Golgi staining showed a significantly reduced total spine density and mature type mushroom spine in S810R ($n = 4$ independent experiments). (**G** and **H**) Effect of the S810R variant on cerebral glucose metabolism evaluated by dynamic PET scans (FDG). (**I**–**M**) Effect of the S810R variant on motor coordination [rotarod, **I**; locomotion, **J**; recognition memory (novel object recognition, NOR; **K**); spatial learning (Y-maze; **L**); and anxiety level (EZM test; **M**)]. (**N**) Effect of the S810R variant on the seizure threshold (PTZ). EZM = elevated zero maze; GTCS = generalized tonic–clonic seizures; MJ = myoclonic jerk; PTZ = pentylenetetrazole. Student's unpaired *t*-test, $^{*}P < 0.05$.

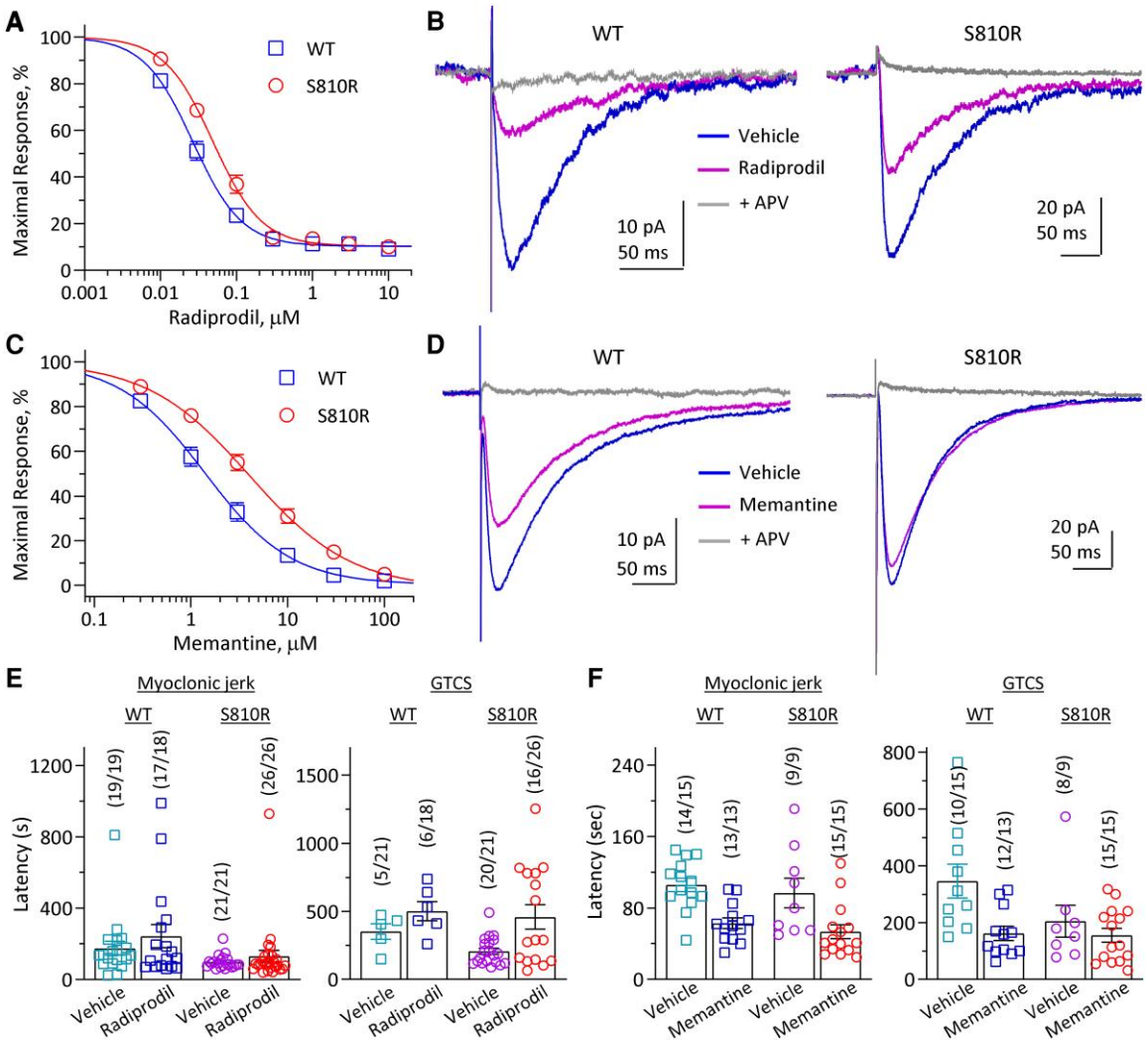

Figure 5 Effects of radiprodil and memantine on agonist-evoked GluN2B NMDAR currents, evoked NMDAR-mediated EPSCs and seizure threshold. (**A** and **C**) Composite concentration–response curves for radiprodil (**A**) and memantine (**C**) at a holding potential of −40 mV assessed by the two-electrode voltage-clamp current recordings from *Xenopus* oocytes expressing GluN1/GluN2B and GluN1/GluN2B-S810R. (**B** and **D**) Effects of radiprodil (**B**; 3 μM) and memantine (**D**; 30 μM) on evoked NMDAR-mediated EPSCs for wild-type (WT) and GluN2B-S810R were recorded from CA1 pyramidal cells in response to Schaffer collateral stimulation in the presence of the AMPA receptor antagonist NBQX (10 μM for GluN2B-S810R) and reduced extracellular Mg^{2+} (0.2 mM). (**E** and **F**) Effect of radiprodil (3.0 mg/kg, i.p.) and memantine (20 mg/kg, i.p.) on the latency to the first myoclonic jerk (MJ) or generalized tonic–clonic seizures (GTCS) induced by pentylenetetrazole (PTZ; 40 mg/kg, i.p.).

travel distance in the open field (locomotion), percentage of novelty preference (NOR) and percentage of correct alternation (Y-maze) between WT mice and those harbouring the *GRIN2B* variant. However, the GluN2B-S810R mice showed altered habituation distances (NOR; Fig. 4K, right) and maze entries (Y-maze; Fig. 4L, right). This might reflect that the knock-in mice might have a high level of anxiety. Indeed, the GluN2B-S810R mice presented a trend of a reduced numbers of open arm crossing (4.1 ± 1.1, versus 7.1 ± 1.7 in WT) and less time spent in the open arm (33 ± 7.5 s, versus 47 ± 7.9 s in WT) of the elevated zero maze test (Table 3 and Fig. 4M), although both changes did not reach statistical significance (P = 0.0932 and P = 0.0588, respectively; Mann–Whitney U-test).

Adult heterozygous male mice often showed generalized seizures (stage IV) when their cage lids were opened (Supplementary Videos 1 and 2; the S801R mouse showed generalized seizures that progressed from repetitive head bobbing to rearing and falling). We therefore evaluated seizure susceptibility by measuring the latency to the initiation of myoclonic jerks and GTCS following intraperitoneal injection of 35 mg/kg of PTZ in 10 WT and 10 GluN2B-S810R female mice (age 14–25 weeks). All mice showed myoclonic jerks, with the GluN2B-S810R mice showing a shorter latency to the first myoclonic jerk (58 ± 1.6 s, versus 115 ± 4.4 s in WT; Table 3 and Fig. 4N). All the S810R mice (10/10) showed GTCS, whereas only half of the WT mice (5/10) progressed to GTCS, with longer latency than variant knock-in mice (183 ± 7.2 s, versus 309 ± 18 s in WT; Table 3 and Fig. 4N). These data suggest that the adult heterozygous GluN2B-S810R mice have a higher seizure susceptibility (i.e. a reduced seizure threshold).

We next determined whether the GluN2B-selective radiprodil can mitigate the altered receptor function caused by the GluN2B-S810R variant. NMDARs containing the GluN2B-S810R variant showed a modestly elevated radiprodil IC_{50} value compared with WT NMDARs (20 nM, versus 53 nM for the WT; Table 2 and Fig. 5A), suggesting that this variant has a comparable sensitivity to radiprodil. We then evaluated whether the evoked NMDAR-mediated EPSCs were sensitive to radiprodil. Our data suggest

that 3 μM radiprodil can significantly inhibit the NMDAR-mediated component of evoked EPSCs in both knock-in GluN2B-S810R and WT CA1 pyramidal cells (Fig. 5B and Table 3). To investigate whether NMDAR antagonists can rectify the reduced seizure threshold in the heterozygous mice harbouring the GluN2B-S810R variant, we initially administered radiprodil (3.0 mg/kg, i.p.) or vehicle to the GluN2B-S810R knock-in mice, which was followed 30 min later by PTZ administration (40 mg/kg, i.p.). There was no significant difference in the latency to the first myoclonic jerk between the vehicle and the radiprodil groups (131 ± 33 s, $n = 26$, versus 99 ± 8.4 s, $n = 21$ of vehicle/control; $P = 0.40$, Student's unpaired *t*-test; Fig. 5E, left and Table 3). Most vehicle-treated GluN2B-S810R mice (20/21) underwent GTCSs at this dose of PTZ, with a latency of 207 ± 23 s following intraperitoneal injection, and 16 of 26 GluN2B-S810R mice treated with radiprodil showed GTCS. The latency to GTCS (458 ± 90 s) was significantly longer in these 16 mice compared with the GluN2B-S810R mice treated with vehicle ($P = 0.0053$, Student's unpaired *t*-test; Fig. 5E, right and Table 3). However, the durations of the PTZ-induced first GTCS are comparable between the vehicle- and radiprodil-treatment groups for both WT and GluN2B-S810R mice (WT, 23 ± 3.0 s for vehicle and 21 ± 0.8 s for radiprodil, $P = 0.47$; GluN2B-S810R, 16 ± 0.9 s for vehicle and 18 ± 1.9 s for radiprodil, $P = 0.34$; Student's unpaired *t*-test).

For a comparison, we tested whether the GluN2B-S810R variant changes the sensitivity to memantine using recordings from both oocytes expressing recombinant NMDARs and evoked EPSCs in CA1 pyramidal cells. The oocyte data showed that the GluN2B-S810R variant led to only a modest reduction in memantine potency (increased IC_{50} value) by 2.9-fold (1.4 μM, versus 4.1 μM in the WT; Fig. 5C). However, patch-clamp data obtained from CA1 pyramidal cells in hippocampal slices suggested that 10 μM memantine did not inhibit the NMDAR-mediated EPSCs in GluN2B-S810R mice (Fig. 5D). We subsequently administered memantine (20 mg/kg body weight, i.p.) or vehicle to the GluN2B-S810R knock-in mice 30 min before PTZ administration. Memantine-treated mice showed a trend to reduce the latency to the first myoclonic jerk (53 ± 2.0 s, $n = 15$; versus vehicle group, 97 ± 5.5 s, $n = 9$; $P = 0.014$, Student's unpaired *t*-test) and first GTCS in GluN2B-S810R mice (156 ± 6.3 s, $n = 15$; versus vehicle group, 205 ± 20 s, $n = 8$; $P = 0.36$, Student's unpaired *t*-test; Fig. 5F). These data suggest that memantine does not mitigate seizure activity in GluN2B-S810R mice and might sensitize mice to PTZ-induced seizures.

Discussion

Here, we show that radiprodil can selectively inhibit NMDARs that contain two copies of GluN2B or a single copy of GluN2B and one copy of either GluN2A, GluN2C or GluN2D. As observed for other GluN2B-selective antagonists,[32,39,59,73] for triheteromeric receptors that contain only one copy of GluN2B, we found reduced potency of radiprodil and reduced overall inhibition at saturating concentrations. We also showed that radiprodil enhanced the potency of glutamate, and although this effect could be manifested as potentiating actions at very low concentrations of agonists,[74] we could not detect any potentiation of NMDAR response amplitude by radiprodil. One might predict inhibitory actions at synaptic receptors that are exposed to saturating concentrations of glutamate following synaptic release. In contrast, depending on the glutamate concentration present at extracellular non-synaptic sites, radiprodil might both increase receptor occupancy and produce a decrease in open probability, with a net effect of diminished inhibition of extracellular GluN2B-containing NMDARs. This is in contrast to what has been reported for ifenprodil, which can enhance the NMDAR response amplitude at very low agonist concentrations.[74] The ramifications of this effect on circuit function have not been explored fully but could be therapeutically important.

We also describe the binding site and pose for radiprodil at 2.74 Å, and these data reveal the following features. Radiprodil binds at the subunit interface between the GluN1 and GluN2B NTDs and has extensive hydrophobic and hydrophilic interactions with residues from the R1 and R2 lobes, respectively. The mode of hydrophobic interactions is more similar to ifenprodil than to EU93-31,[63] whereas that of hydrophilic interactions is more similar to EU93-31 than to ifenprodil, harbouring two polar interactions with the R2 lobe residues. Radiprodil would have higher inhibitory capability in comparison to ifenprodil, owing to stronger interactions with the R2 lobe residues to favour the closure of the GluN2B NTD bi-lobes, which, in turn, stabilizes the non-active-like conformation in the context of the intact receptors.[64,66] Interestingly, radiprodil inhibition is relatively insensitive to extracellular pH, which is different from context-dependent GluN2B antagonists, such as EU93-31[75] and NP10679.[76]

Rare *de novo GRIN1* and *GRIN2B* missense variants appear to be associated with a number of neurological conditions, some of which can produce a strong GoF that is associated with epilepsy.[17,18,67] Evaluation of the effect of these variants on radiprodil potency is instructive because it shows that the allosteric inhibition imparted by stabilization of the heterodimer interface and associated closure of the bi-lobed NTD can inhibit NMDARs that contained variants in most domains. This suggests that the control of gating imparted by the NTD remains intact even when variants reside in the transmembrane domain, gating motifs, linkers or agonist binding domains and influence channel function. However, ~20% of the variants tested show either diminished potency and/or diminished inhibition at saturating radiprodil concentrations; one variant was largely insensitive to radiprodil (Table 2).

We also describe a mouse model in which we have knocked in a GoF *GRIN2B* variant (Ser810Arg) associated with intractable seizures and early-onset epileptic encephalopathy. The variant significantly enhances NMDAR function by elevating agonist potency (for both glutamate and glycine), reducing proton inhibition, prolonging synaptic-like response time course and increasing channel open probability. These *in vitro* data suggest that the S810R variant produces a strong GoF variant. These heterozygous mice show reduced total dendritic spine density and a reduction in mature mushroom spines, suggesting that this variant might impair spine maturation. We also observed an increase in the amplitude of NMDAR-mediated synaptic responses. The adult heterozygous mice showed spontaneous generalized seizures (stage IV) when the cage lids were lifted and presented a higher susceptibility to chemoconvulsant-induced seizures (i.e. a reduced seizure threshold). The adult heterozygous mice showed reduced cerebral glucose metabolism (i.e. decreased FDG signal level in PET scans), which is consistent with the PET data on human epileptic patients.[77] These data suggest that the heterozygous GluN2B-S810R mice can mimic the seizure phenotype of patients.

Finally, we evaluated the ability of radiprodil to mitigate the altered synaptic activity and reduce seizure sensitivity in adult heterozygous GluN2B-S810R mice. We found that radiprodil can significantly reduce the enhanced current amplitude of eEPSCs in brain slices from the mice that contain the GluN2B-S810R variant and prolong the time to seizure onset following introduction of

the chemoconvulsant pentylene tetrazole. However, memantine, a US Food and Drug Administration-approved NMDAR channel blocker, is generally less efficacious than radiprodil for this variant and appears to sensitize mice to PTZ-induced seizures. It is well known that memantine has a relatively higher affinity/potency for GluN2D-containing NMDARs than the receptors that contain GluN2A or GluN2B.[78] GluN2D is expressed predominantly in certain types of hippocampal and cortical interneurons and contributes to the activation of these interneurons, which enhances the inhibitory output of interneurons to pyramidal cells.[79-83] Preference of memantine inhibition on GluN2D-expressing interneurons (e.g. parvalbumin-positive) could further exacerbate the imbalance of excitation–inhibition caused by the GluN2B-S810R variant. These data support the possibility that GluN2B-selective allosteric antagonists could have utility in forms of epilepsy that involve overactivation of GluN2B receptors.

Conclusion

Here, we show that radiprodil can inhibit NMDARs that contain a single copy or two copies of GluN2B with high potency and selectivity, and it is an effective antagonist at multiple human *GRIN1* and *GRIN2B* missense variants related to various neurological and neuropsychiatric conditions. The X-ray crystallography data demonstrate the binding site and pose for radiprodil at the subunit interface between the GluN1 and GluN2B NTDs. Inhibition of GluN2B-containing NMDARs by radiprodil might be achieved by stabilizing the non-active-like conformation and facilitating the closure of the GluN2B NTD bi-lobes through strong interactions with the R2 lobe residues. Furthermore, radiprodil can mitigate the altered synaptic activity and decrease seizure sensitivity in a knock-in mouse line harbouring a GoF *GRIN2B* variant associated with early-onset epileptic encephalopathy, suggesting its potential use in personalized medicine.

Data availability

Data presented in this publication are available for sharing upon request from the academic research community. All novel DNAs and animal models designed and created in this publication are made available, free of charge, to the academic research community upon request under the typical academic material transfer agreement. The structural coordinate for GluN1b–GluN2B NTD in complex with radiprodil has been deposited to the Protein Data Bank under the accession code 9Q3Y.

Acknowledgements

We thank Dr Ray Dingledine for critical comments on the manuscript, Dr Nicholas Varvel for his valuable assistance in reviewing and interpreting the video recordings of the mouse seizure activity, and Kelsey Nocilla for excellent technical assistance, in addition to Dr Jason Schroeder and Emory University Rodent Behavioral Core (RRID:SCR_012499) for behavioural tests.

Funding

This work was supported by the National Institute of Neurological Disorders and Stroke (NS111619 S.F.T., NS111745 H.F. and 113632 H.F.), the National Institute of Mental Health (MH085926 H.F. and MH127404 H.Y.), the Eunice Kennedy Shriver National Institute of Child Health and Human Development (HD082373 H.Y.), National Institute on Aging (AG072142 S.J.M., AG075444 S.H.L., AG080262 S.H.L. and AG083084 S.H.L.), National Institute of Biomedical Imaging and Bioengineering (S10OD034326 S.H.L.), the GRIN2B Foundation (H.Y.), GRIN Therapeutics (S.F.T. and S.J.M.), Austin's Purpose (S.F.T. and H.F.), SFARI (732132 to S.F.T.), Robertson funds at Cold Spring Harbor Laboratory (H.F.), Doug Fox Alzheimer's fund (H.F.), Heartfelt Wing Alzheimer's fund (H.F.), the Gertrude and Louis Feil Family Trust (H.F.), by Imagine, Innovate and Impact (I^3) Awards from the Emory University School of Medicine and through the Georgia CTSA NIH award (UL1-TR002378; H.Y. and S.H.L.), ODPRT, NUS (C.-M.L.). This research was supported in part by the Intramural Research Program of the National Institutes of Health (NIH) . The contributions of the NIH authors (S.W. and K.W.R.) were made as part of their official duties as NIH federal employees, are in compliance with agency policy requirements, and are considered Works of the United States Government. However, the findings and conclusions presented in this paper are those of the authors and do not necessarily reflect the views of the NIH or the U.S. Department of Health and Human Services.

Competing interests

The authors declare the following competing interest(s): S.F.T. is a member of the SAB for Eumentis Therapeutics, Neurocrine Biosciences, a member of the MAB for the GRIN2B Foundation and the CureGRIN Foundation, a consultant for GRIN Therapeutics, Seyltx and Sage Therapeutics, a co-founder of NeurOp Inc. and AgriThera, and a member of the Board of Directors for NeurOp Inc. S.F.T. is Principal Investigator of a grant from GRIN Therapeutics, and H.Y. is Principal Investigator of a grant from Sage Therapeutics.

Supplementary material

Supplementary material is available at *Brain* online.

References

1. Hansen KB, Wollmuth LP, Bowie D, et al. Structure, function, and pharmacology of glutamate receptor ion channels. *Pharmacol Rev*. 2021;73:1469–11658.
2. Mayer ML, Westbrook GL, Guthrie PB. Voltage-dependent block by Mg^{2+} of NMDA responses in spinal-cord neurons. *Nature*. 1984;309:261-263.
3. Nowak L, Bregestovski P, Ascher P, Herbet A, Prochiantz A. Magnesium gates glutamate-activated channels in mouse central neurons. *Nature*. 1984;307:462-465.
4. Lau CG, Zukin RS. NMDA receptor trafficking in synaptic plasticity and neuropsychiatric disorders. *Nat Rev Neurosci*. 2007;8:413-426.
5. Mony L, Kew JNC, Gunthorpe MJ, Paoletti P. Allosteric modulators of NR2B-containing NMDA receptors: Molecular mechanisms and therapeutic potential. *Br J Pharmacol*. 2009;157:1301–1317.
6. Traynelis SF, Wollmuth LP, McBain CJ, et al. Glutamate receptor ion channels: Structure, regulation, and function. *Pharmacol Rev*. 2010;62:405-496.
7. Hanson JE, Yuan HJ, Perszyk RE, et al. Therapeutic potential of N-methyl-D-aspartate receptor modulators in psychiatry. *Neuropsychopharmacology*. 2024;49:51-66.

8. Burnashev N, Szepetowski P. NMDA receptor subunit mutations in neurodevelopmental disorders. *Curr Opin Pharmacol*. 2015;20:73-82.
9. Yuan H, Low CM, Moody OA, Jenkins A, Traynelis SF. Ionotropic GABA and glutamate receptor mutations and human neurologic diseases. *Mol Pharmacol*. 2015;88:203-217.
10. Hu C, Chen W, Myers SJ, Yuan H, Traynelis SF. Human *GRIN2B* variants in neurodevelopmental disorders. *J Pharmacol Sci*. 2016;132:115-121.
11. Li D, Yuan H, Ortiz-Gonzalez XR, et al. *GRIN2D* recurrent de novo dominant mutation causes a severe epileptic encephalopathy treatable with NMDA receptor channel blockers. *Am J Hum Genet*. 2016;99:802-816.
12. Swanger SA, Chen W, Wells G, et al. Mechanistic insight into NMDA receptor dysregulation by rare variants in the GluN2A and GluN2B agonist binding domains. *Am J Hum Genet*. 2016;99:1261-1280.
13. XiangWei W, Jiang Y, Yuan H. *De novo* mutations and rare variants occurring in NMDA receptors. *Curr Opin Physiol*. 2018;2:27-35.
14. XiangWei W, Kannan V, Xu Y, et al. Heterogeneous clinical and functional features of *GRIN2D*-related developmental and epileptic encephalopathy. *Brain*. 2019;142:3009-3027.
15. Myers SJ, Yuan H, Kang JQ, Tan FCK, Traynelis SF, Low CM. Distinct roles of *GRIN2A* and GRIN2B variants in neurological conditions. *F1000Res*. 2019;8:1940.
16. Strehlow V, Heyne HO, Vlaskamp DRM, et al. *GRIN2A*-related disorders: Genotype and functional consequence predict phenotype. *Brain*. 2019;142:80-92.
17. Benke TA, Park K, Krey I, et al. Clinical and therapeutic significance of genetic variation in the *GRIN* gene family encoding NMDARs. *Neuropharmacology*. 2021;199:108805.
18. Xu YC, Song R, Perszyk RE, et al. De novo *GRIN* variants in M3 helix associated with neurological disorders control channel gating of NMDA receptor. *Cell Mol Life Sci*. 2024;81:153.
19. Addis L, Virdee JK, Vidler LR, Collier DA, Pal DK, Ursu D. Epilepsy-associated *GRIN2A* mutations reduce NMDA receptor trafficking and agonist potency – Molecular profiling and functional rescue. *Sci Rep*. 2017;7:66.
20. Vyklicky V, Krausova B, Cerny J, et al. Surface expression, function, and pharmacology of disease-associated mutations in the membrane domain of the human GluN2B subunit. *Front Mol Neurosci*. 2018;11:110.
21. Santos-Gomez A, Miguez-Cabello F, Garcia-Recio A, et al. Disease-associated GRIN protein truncating variants trigger NMDA receptor loss-of-function. *Hum Mol Genet*. 2021;29:3859-3871.
22. Xie LMM, Perszyk RE, Kim S, et al. Functional effects of disease-associated variants reveal that the S1–M1 linker of the NMDA receptor critically controls channel opening. *Cell Mol Life Sci*. 2023;80:110.
23. Moody G, Musco A, Bennett J, Wollmuth LP. An integrated approach to evaluate the functional effects of disease-associated NMDA receptor variants. *Neuropharmacology*. 2023;240:109703.
24. Myers SJ, Yuan HJ, Perszyk RE, et al. Classification of missense variants in the N-methyl-D-aspartate receptor *GRIN* gene family as gain- or loss-of-function. *Hum Mol Genet*. 2023;32:2857-2871.
25. Burnell ES, Irvine M, Fang GY, Sapkota K, Jane DE, Monaghan DT. Positive and negative allosteric modulators of *N*-methyl-D-aspartate (NMDA) receptors: Structure–activity relationships and mechanisms of action. *J Med Chem*. 2019;62:3-23.
26. Patat A, Molinier P, Hergueta T, et al. Lack of amnestic, psychotomimetic or impairing effect on psychomotor performance of eliprodil, a new NMDA antagonist. *Int Clin Psychopharm*. 1994;9:155-162.
27. Yurkewicz L, Weaver J, Bullock MR, Marshall LF. The effect of the selective NMDA receptor antagonist traxoprodil in the treatment of traumatic brain injury. *J Neurotrauma*. 2005;22:1428-1443.
28. Herring WJ, Assaid C, Budd K, et al. A phase Ib randomized controlled study to evaluate the effectiveness of a single-dose of the NR2B selective *N*-methyl-D-aspartate antagonist MK-0657 on levodopa-induced dyskinesias and motor symptoms in patients with Parkinson disease. *Clin Neuropharmacol*. 2017;40:255-260.
29. Auvin S, Dozieres-Puyravel B, Avbersek A, et al. Radiprodil, a NR2B negative allosteric modulator, from bench to bedside in infantile spasm syndrome. *Ann Clin Transl Neurol*. 2020;7:343-352.
30. Sasaki T, Hashimoto K, Niitsu T, et al. Ifenprodil tartrate treatment of adolescents with post-traumatic stress disorder: A double-blind, placebo-controlled trial. *Psychiatry Res*. 2022;311:114486.
31. Zaczek R, Traynelis SF, Dingledine R, Koszalka GW, Laskowitz DT. Phase 1 clinical results for NP10679, a pH-sensitive GluN2B-selective *N*-methyl-D-aspartate receptor inhibitor. *Clin Pharmacol Drug Dev*. 2023;12:706-717.
32. Hansen KB, Ogden KK, Yuan HJ, Traynelis SF. Distinct functional and pharmacological properties of triheteromeric GluN1/GluN2A/GluN2B NMDA receptors. *Neuron*. 2014;81:1084-1096.
33. Strong KL, Epplin MP, Ogden KK, et al. Distinct GluN1 and GluN2 structural determinants for subunit-selective positive allosteric modulation of *N*-methyl-D-aspartate receptors. *ACS Chem Neurosci*. 2021;12:79-98.
34. Yi F, Traynelis SF, Hansen KB. Selective cell-surface expression of triheteromeric NMDA receptors. *Methods Mol Biol*. 2024;2799:55-77.
35. Jackson MR, Nilsson T, Peterson PA. Identification of a consensus motif for retention of transmembrane proteins in the endoplasmic reticulum. *EMBO J*. 1990;9:3153-3162.
36. Jackson MR, Nilsson T, Peterson PA. Retrieval of transmembrane proteins to the endoplasmic reticulum. *J Cell Biol*. 1993;121:317-333.
37. Zerangue N, Malan MJ, Fried SR, et al. Analysis of endoplasmic reticulum trafficking signals by combinatorial screening in mammalian cells. *Proc Natl Acad Sci U S A*. 2001;98:2431-2436.
38. Bhattacharya S, Khatri A, Swanger SA, et al. Triheteromeric GluN1/GluN2A/GluN2C NMDARs with unique single-channel properties are the dominant receptor population in cerebellar granule cells. *Neuron*. 2018;99:315-328.e5.
39. Yi F, Bhattacharya S, Thompson CM, Traynelis SF, Hansen KB. Functional and pharmacological properties of triheteromeric GluN1/2B/2D NMDA receptors. *J Physiol*. 2019;597:5495-5514.
40. Chen C, Okayama H. High-efficiency transformation of mammalian cells by plasmid DNA. *Mol Cell Biol*. 1987;7:2745-2752.
41. Traynelis SF, Burgess MF, Zheng F, Lyuboslavsky P, Powers JL. Control of voltage-independent zinc inhibition of NMDA receptors by the NR1 subunit. *J Neurosci*. 1998;18:6163-6175.
42. Karakas E, Simorowski N, Furukawa H. Structure of the zinc-bound amino-terminal domain of the NMDA receptor NR2B subunit. *EMBO J*. 2009;28:3910-3920.
43. Karakas E, Simorowski N, Furukawa H. Subunit arrangement and phenylethanolamine binding in GluN1/GluN2B NMDA receptors. *Nature*. 2011;475:249-253.
44. Mccoy AJ, Grosse-Kunstleve RW, Adams PD, Winn MD, Storoni LC, Read RJ. *Phaser* crystallographic software. *J Appl Crystallogr*. 2007;40:658-674.
45. Emsley P, Lohkamp B, Scott WG, Cowtan K. Features and development of *Coot*. *Acta Crystallogr D Biol Crystallogr*. 2010;66:486-501.
46. Won S, Incontro S, Nicoll RA, Roche KW. PSD-95 stabilizes NMDA receptors by inducing the degradation of STEP. *Proc Natl Acad Sci U S A*. 2016;113:E4736-E4744.

47. Won S, Incontro S, Li Y, Nicoll RA, Roche KW. The $STEP_{61}$ interactome reveals subunit-specific AMPA receptor binding and synaptic regulation. *Proc Natl Acad Sci U S A*. 2019;116:8028-8037.
48. Michel A, Downey P, Nicolas JM, Scheller D. Unprecedented therapeutic potential with a combination of A_{2A}/NR2B receptor antagonists as observed in the 6-OHDA lesioned rat model of Parkinson's disease. *PLoS One*. 2014;9:e114086.
49. Fernandes A, Wojcik T, Baireddy P, et al. Inhibition of in vivo [^{3}H]MK-801 binding by NMDA receptor open channel blockers and GluN2B antagonists in rats and mice. *Eur J Pharmacol*. 2015;766:1-8.
50. Chazot PL, Coleman SK, Cik M, Stephenson FA. Molecular characterization of *N*-methyl-D-aspartate receptors expressed in mammalian cells yields evidence for the coexistence of three subunit types within a discrete receptor molecule.. *J Biol Chem*. 1994;269:24403-24409.
51. Sheng M, Cummings J, Roldan LA, Jan YN, Jan LY. Changing subunit composition of heteromeric NMDA receptors during development of rat cortex. *Nature*. 1994;368:144-147.
52. Luo JH, Wang YH, Yasuda RP, Dunah AW, Wolfe BB. The majority of *N*-methyl-D-aspartate receptor complexes in adult rat cerebral cortex contain at least three different subunits (NR1/NR2A/NR2B). *Mol Pharmacol*. 1997;51:79-86.
53. Al-Hallaq RA, Conrads TP, Veenstra TD, Wenthold RJ. NMDA diheteromeric receptor populations and associated proteins in rat hippocampus. *J Neurosci*. 2007;27:8334-8343.
54. Rauner C, Köhr G. Triheteromeric NR1/NR2A/NR2B receptors constitute the major N-methyl-D-aspartate receptor population in adult hippocampal synapses. *J Biol Chem*. 2011;286:7558-7566.
55. Tovar KR, McGinley MJ, Westbrook GL. Triheteromeric NMDA receptors at hippocampal synapses. *J Neurosci*. 2013;33:9150–9160.
56. Stroebel D, Carvalho S, Grand T, Zhu S, Paoletti P. Controlling NMDA receptor subunit composition using ectopic retention signals. *J Neurosci*. 2014;34:16630-16636.
57. Sun WN, Hansen KB, Jahr CE. Allosteric interactions between NMDA receptor subunits shape the developmental shift in channel properties. *Neuron*. 2017;94:58-64.e3.
58. Han W, Yuan H, Allen JP, et al. Opportunities for precision treatment of *GRIN2A* and *GRIN2B* gain-of-function variants in triheteromeric N-methyl-D-aspartate receptors. *J Pharmacol Exp Ther*. 2022;381:54-66.
59. Hatton CJ, Paoletti P. Modulation of triheteromeric NMDA receptors by N-terminal domain ligands. *Neuron*. 2005;46:261-274.
60. Regan MC, Grant T, McDaniel MJ, et al. Structural mechanism of functional modulation by gene splicing in NMDA receptors. *Neuron*. 2018;98:521-529.e3.
61. Karakas E, Furukawa H. Crystal structure of a heterotetrameric NMDA receptor ion channel. *Science*. 2014;344:992-997.
62. Lee CH, Lu W, Michel JC, et al. NMDA receptor structures reveal subunit arrangement and pore architecture. *Nature*. 2014;511:191-197.
63. Regan MC, Zhu ZJ, Yuan HJ, et al. Structural elements of a pH-sensitive inhibitor binding site in NMDA receptors. *Nat Commun*. 2019;10:321.
64. Chou TH, Tajima N, Romero-Hernandez A, Furukawa H. Structural basis of functional transitions in mammalian NMDA receptors. *Cell*. 2020;182:357-371.e13.
65. Chou TH, Kang H, Simorowski N, Traynelis SF, Furukawa H. Structural insights into assembly and function of GluN1-2C, GluN1-2A-2C, and GluN1-2D NMDARs. *Mol Cell*. 2022;82:4548-4563.e4.
66. Tajima N, Karakas E, Grant T, et al. Activation of NMDA receptors and the mechanism of inhibition by ifenprodil. *Nature*. 2016;534:63-68.
67. Platzer K, Yuan H, Schutz H, et al. *GRIN2B* encephalopathy: Novel findings on phenotype, variant clustering, functional consequences and treatment aspects. *J Med Genet*. 2017;54:460-470.
68. Mullier B, Wolff C, Sands ZA, et al. GRIN2B gain of function mutations are sensitive to radiprodil, a negative allosteric modulator of GluN2B-containing NMDA receptors. *Neuropharmacology*. 2017;123:322-331.
69. Yuan H, Hansen KB, Zhang J, et al. Functional analysis of a *de novo GRIN2A* missense mutation associated with early-onset epileptic encephalopathy. *Nat Commun*. 2014;5:3251.
70. Chen W, Tankovic A, Burger PB, Kusumoto H, Traynelis SF, Yuan H. Functional evaluation of a de novo *GRIN2A* mutation identified in a patient with profound global developmental delay and refractory epilepsy. *Mol Pharmacol*. 2017;91:317-330.
71. Ogden KK, Chen W, Swanger SA, et al. Molecular mechanism of disease-associated mutations in the pre-M1 helix of NMDA receptors and potential rescue pharmacology. *PLoS Genet*. 2017;13:e1006536.
72. Perszyk RE, Myers SJ, Yuan H, et al. Hodgkin–Huxley–Katz Prize Lecture: Genetic and pharmacological control of glutamate receptor channel through a highly conserved gating motif. *J Physiol*. 2020;598:3071–33083.
73. Stroebel D, Buhl DL, Knafels JD, et al. A novel binding mode reveals two distinct classes of NMDA receptor GluN2B-selective antagonists. *Mol Pharmacol*. 2016;89:541-551.
74. Kew JNC, Trube G, Kemp JA. A novel mechanism of activity-dependent NMDA receptor antagonism describes the effect of ifenprodil in rat cultured cortical neurones. *J Physiol*. 1996;497:761-772.
75. Yuan H, Myers SJ, Wells G, et al. Context-dependent GluN2B-selective inhibitors of NMDA receptor function are neuroprotective with minimal side effects. *Neuron*. 2015;85:1305–1318.
76. Myers SJ, Ruppa KP, Wilson LJ, et al. A glutamate *N*-methyl-D-aspartate (NMDA) receptor subunit 2B-selective inhibitor of NMDA receptor function with enhanced potency at acidic pH and oral bioavailability for clinical use. *J Pharmacol Exp Ther*. 2021;379:41-52.
77. Sarikaya I. PET studies in epilepsy. *Am J Nucl Med Mol Imaging*. 2015;5:416-430.
78. Kotermanski SE, Johnson JW. Mg^{2+} imparts NMDA receptor subtype selectivity to the Alzheimer's drug memantine. *J Neurosci*. 2009;29:2774-2779.
79. Booker SA, Sumera A, Kind PC, Wyllie DJA. Contribution of NMDA receptors to synaptic function in rat hippocampal interneurons. *eNeuro*. 2021;8:ENEURO.0552-20.2021.
80. Perszyk RE, DiRaddo JO, Strong KL, et al. GluN2D-containing N-methyl-D-aspartate receptors mediate synaptic transmission in hippocampal interneurons and regulate interneuron activity. *Mol Pharmacol*. 2016;90:689-702.
81. Swanger SA, Vance KM, Acker TM, et al. A novel negative allosteric modulator selective for GluN2C/2D-containing NMDA receptors inhibits synaptic transmission in hippocampal interneurons. *ACS Chem Neurosci*. 2018;9:306-319.
82. Köhler I, Rennau LM, Hoffmann L, et al. Activation of GluN2D-containing NMDA receptors promotes development of axons and axon-carrying dendrites of cortical interneurons. *Cereb Cortex*. 2025;35:bhaf136.
83. Camp CR, Banke TG, Xing H, et al. Selective enhancement of the interneuron network and gamma-band power via GluN2C/GluN2D NMDA receptor potentiation. *J Physiol*. 2025;603:4027-4049.